

PAPER • OPEN ACCESS

The 2021 release of the Quantemol database (QDB) of plasma chemistries and reactions

To cite this article: Jonathan Tennyson *et al* 2022 *Plasma Sources Sci. Technol.* **31** 095020

View the [article online](#) for updates and enhancements.

You may also like

- [Suppressor Effects during Copper Superfilling of Sub- 100 nm Lines](#)
Q. Huang, B. C. Baker-O'Neal, J. J. Kelly *et al.*
- [High-Voltage Metal-Free Disproportionation Flow Batteries Based on 9,10-diphenylanthracene](#)
James D. Saraidaridis, James A. Suttill and Charles W. Monroe
- [Calculated cross sections for electron collisions with \$NF_3\$, \$NF_2\$, and \$NF\$ with applications to remote plasma sources](#)
James R Hamilton, Jonathan Tennyson, Shuo Huang *et al.*



HIDEN ANALYTICAL

Analysis Solutions for your Plasma Research

- Knowledge,
- Experience,
- Expertise

[Click to view our product catalogue](#)

Contact Hiden Analytical for further details:
W www.HidenAnalytical.com
E info@hiden.co.uk



Surface Science

- ▶ Surface Analysis
- ▶ SIMS



3D depth Profiling

- ▶ 3D depth Profiling
- ▶ Nanometre depth resolution



Plasma Diagnostics

- ▶ Plasma characterisation
- ▶ Customised systems to suit plasma Configuration



Mass and energy analysis of plasma ions

- ▶ Mass and energy analysis of plasma ions
- ▶ Characterisation of neutrals and radicals

The 2021 release of the Quantemol database (QDB) of plasma chemistries and reactions

Jonathan Tennyson^{1,*} , Sebastian Mohr², M Hanicinea¹ , Anna Dzarasova², Carrick Smith² , Sarah Waddington², Bingqing Liu¹, Luís L Alves³ , Klaus Bartschat⁴ , Annemie Bogaerts⁵ , Sebastian U Engelmann⁶, Timo Gans^{7,13} , Andrew R Gibson^{8,9} , Satoshi Hamaguchi¹⁰ , Kathryn R Hamilton⁴ , Christian Hill¹¹ , Deborah O'Connell^{7,13}, Shahid Rauf¹² , Kevin van 't Veer⁵  and Oleg Zatsarinny^{4,†} 

¹ Department of Physics and Astronomy, University College, London, Gower St., London WC1E 6BT, United Kingdom

² Quantemol Ltd., 320 City Rd, London EC1V 2NZ, United Kingdom

³ Instituto de Plasmas e Fusão Nuclear, Instituto Superior Técnico, Universidade de Lisboa, Av Rovisco Pais 1049-001 Lisboa, Portugal

⁴ Department of Physics and Astronomy, Drake University, IA 50311, United States of America

⁵ Research group PLASMANT, University of Antwerp, Belgium

⁶ IBM T J Watson Research Center, Yorktown Heights, NY 10598, United States of America

⁷ National Centre for Plasma Science Technology, Dublin City University, Dublin, Ireland

⁸ Research Group for Biomedical Plasma Technology, Ruhr-Universität Bochum, Germany

⁹ Institute of Electrical Engineering and Plasma Technology, Ruhr-Universität Bochum, Germany

¹⁰ Center for Atomic and Molecular Technologies, Graduate School of Engineering, Osaka University, Japan

¹¹ Atomic and Molecular Data Unit, Division of Physical and Chemical Sciences, International Atomic Energy Agency, Vienna, Austria

¹² Applied Materials Inc., Sunnyvale, CA 94085, United States of America

¹³ School of Physical Sciences, Faculty of Science and Health, Dublin City University, Dublin, Ireland

E-mail: j.tennyson@ucl.ac.uk

Received 22 December 2021, revised 31 July 2022

Accepted for publication 8 September 2022

Published 9 December 2022




Abstract

The Quantemol database (QDB) provides cross sections and rates of processes important for plasma models; heavy particle collisions (chemical reactions) and electron collision processes are considered. The current version of QDB has data on 28 917 processes between 2485 distinct species plus data for surface processes. These data are available via a web interface or can be delivered directly to plasma models using an application program interface; data are available in formats suitable for direct input into a variety of popular plasma modeling codes including HPPEM, COMSOL, ChemKIN, CFD-ACE+, and VisGlow. QDB provides ready assembled plasma chemistries plus the ability to build bespoke chemistries. The database also provides a Boltzmann solver for electron dynamics and a zero-dimensional model. These

* Author to whom any correspondence should be addressed.

† Deceased.

 Original content from this work may be used under the terms of the [Creative Commons Attribution 4.0 licence](https://creativecommons.org/licenses/by/4.0/). Any further distribution of this work must maintain attribution to the author(s) and the title of the work, journal citation and DOI.

developments, use cases involving O₂, Ar/NF₃, Ar/NF₃/O₂, and He/H₂O/O₂ chemistries, and plans for the future are presented.

Keywords: atomic and molecular data, chemistries, plasma models, low temperature plasmas

(Some figures may appear in colour only in the online journal)

1. Introduction

The extensive use of plasma processes has become a major driver in technological and scientific development. Many of these plasmas are cold in the sense that they possess significant molecular content. Constructing detailed models for cold plasmas is important for both understanding and driving future developments in the field [1]. These models require accurate and comprehensive reaction datasets of atomic, molecular and other processes. As a result a number of databases are being actively developed. These include LXCat [2], which concentrates on electron collision data, recently updated databases from the Japanese National Institute for Fusion Science [3] and the Korean National Fusion Research Institute [4] (now called the Korea Institute of Fusion Energy) designed primarily for fusion studies, the kinetic database for astrochemistry (KIDA) [5, 6] and the Phys4Entry database [7] which is primarily designed to model re-entry physics in planetary atmospheres. The Quantemol database (QDB), the subject of the present paper, was designed to meet the needs of plasma modellers by providing data on all processes that could be important in the plasma. These data can then be assembled to give a complete chemistry for the plasma under the relevant conditions. The need for improved modeling capabilities and access to associated data has been identified in recent roadmaps of low temperature plasma science and technology [8, 9].

The original release of QDB [10] comprised 904 species linked by 4099 reactions as well as 29, largely untested, plasma chemistries. In this paper, we report extensive development of the QDB database. The number of species, reactions and chemistries are now increased to 2485, 28 917 and 39, respectively. As discussed below, the data structure for each species has been significantly extended to provide important extra information. In addition, surface processes are now considered and QDB has added functionality in the form of an integrated Boltzmann solver and zero-dimensional chemical model. Data can now be output using an application program interface (API) and in various formats appropriate for commonly used plasma modeling packages. In addition, the number of validated chemistries has increased significantly since the original release; some of these use cases are given as part of this paper.

The paper is structured as follows: section 2 describes the current status of the database including its increased functionality; section 3 presents the new data added to QDB and section 4 gives sample use cases and chemistry reductions. The conclusions in section 5 give some of our plans for future developments of QDB. Some extra information including lists

of species used in QDB and a summary of the main acronyms used in this paper are given as appendices A and B.

2. Database overview

2.1. Data and data structure

The heart of QDB are a series of processes, described as reactions below, which are designed to encapsulate the key steps which lead to changes in the atomic and molecular composition of a plasma. Each reaction involves a set of species which can be either atoms, molecules, a surface or electrons and the result of the reaction a set of products. Within the QDB data structure, there are species and reaction data types. As part of the update the data associated with each species has been significantly extended, see table 1; this is discussed in the next section. Surface processes, also discussed below, have been included which has also led to the extension of the data model.

QDB provides reaction rates, cross sections and chemistries. The basic data item is the species, which can be state-specific. Species include the electron, the photon, and *M*, the third body in three-body reactions, plus 2485 other atomic and molecular species which comprises 938 unstateful species and 1547 stateful species for which each state-specified species is counted separately.

2.2. Species

Atomic and molecular species have characteristics that need to be captured by the database. First, they can be stateful or unstateful. Unstateful species are simply denoted by a chemical formula such as CO for carbon monoxide. Stateful species include the designation of a specific state of the species such as ' $\text{CO } v=10$ ', which means the molecule is in a state with 10 quanta of vibrational excitation or ' $\text{CO } a(3\Pi)$ ' which means CO in its (first) excited electronic state which is of $^3\Pi$ symmetry and is designated as the $a^3\Pi$ state. There are also some data on rotationally excited molecules in which case the rotational states are designated by rotational quantum number *J*. Where possible states are specified using PYVALEM format [11, 12]. For discussion of the notation used to designate the different states of atoms and molecules see references [13, 14]. For many applications having a full set of states is too heavy, so there are also compound excited states which are denoted as, for example, CO* and CO**.

Since the last release these compound states have been made consistent with the individual states. For this, we introduced parent and child states. Parent states are the pooled

Table 1. Data associated with the species data type.

Data	Units	Description
Chemical formula	None	Stoichiometric formula
M	Da	Total atomic mass
q	e	Net charge in units of electron charge
$\Delta_f H^0(298.15)$	eV	Enthalpy of formation at 298.15 K
$\Delta_f H^0(T)$	Various	Enthalpy of formation ^a
S^0	Various	Entropy ^a
$C_p(T)$	Various	Specific heat ^a
LJE (ϵ_{LJ})	K	Lennard-Jones short-range parameter
LJS (σ_{LJ})	Å	Lennard-Jones long-range parameter
α_0	Å ³	Spherical polarisability
IP	eV	Ionisation potential

^aAs represented by a NASA polynomial with user selected units, see text for detail.

states while child states are the individual states. Each parent state can have several child states and vice versa; each individual state can belong, in principle, to more than one pooled state to account for different pooling schemes. Similarly, reactions involving excited states have a parent–child relationship instead of duplicating, for example, the electron impact excitation to the individual states for the excitation to the pooled states. Here however, the electron impact reactions to the individual states as the fundamental processes are the parent reactions. Parent reactions have their own datasets, i.e. cross sections and/or Arrhenius parameters, linked to them. Child reactions, on the other hand, do not have their own datasets but refer to the datasets of the parent reactions.

For example, consider O^* which pools the O^1D and O^1S state. In this scheme:

- O^* act as parent state to O^1D and O^1S .
- The electron impact excitation to O^1D and O^1S are parent reactions to the electron impact excitation to O^* .

The goal of these parent–child relations is to be able to construct chemistry sets with either pooled or individual states without missing reactions or the need to duplicate datasets, and to maintain consistency between the two representations of excited states. For example, when adding O^* to a set, the cross-sectional data for the electron impact excitation will be automatically drawn from the reactions associated with the individual states without the need for the user to manually adjust the reactions. This means that if the user wants to construct an oxygen-containing chemistry set with the chemistry generator (described in detail below) and use the pooled state O^* , the excitation reaction $e + O \rightarrow e + O^*$ will automatically be added with the cross-sectional data for the individual states.

The data associated with each species has been significantly expanded since the original QDB release; these are summarized in table 1. Each species is specified by a simple chemical formula with no distinction made between different isomers so, for example, HCN represents both hydrogen cyanide (HCN) and hydrogen isocyanide (HNC). Where applicable, data refers to the most stable isomer, in this case HCN.

Charge (q) and mass of the given species are straightforward. At present QDB contains 1506 neutral species, 255 species with $q = 1$, 21 with $q = 2$ and 36 with $q = -1$. Tables B1, B3 and B2 in appendix B summarise the neutrals, anions and cations currently considered by QDB, respectively.

Heats or enthalpies of formation, $\Delta_f H^0(298.15)$, are given for room temperature of $T = 298.15$ K and were largely sourced from the active thermochemical tables (ATcT) [15, 16] and JANAF [17], with the more modern ATcT data being given preference. NASA seven-term polynomials [18,19] are used to represent the specific heat at constant pressure, $C_p(T)$, as a function of temperature:

$$\frac{C_p(T)}{R} = \frac{a_1}{T^2} + \frac{a_2}{T} + a_3 + a_4 T + a_5 T^2 + a_6 T^3 + a_7 T^4, \quad (1)$$

where R is the ideal gas constant. These formula are valid in the range $200 \leq T \leq 6000$ K. The coefficients can also be used to represent the temperature dependence of the enthalpy of formation:

$$\frac{\Delta_f H^0}{RT} = a_1 + \frac{a_2}{2} T + \frac{a_3}{3} T^2 + \frac{a_4}{4} T^3 + \frac{a_5}{5} T^4 + \frac{a_6}{T} \quad (2)$$

and entropy

$$\frac{S^0}{RT} = a_1 \ln T + a_2 T + \frac{a_3}{2} T^2 + \frac{a_4}{3} T^3 + \frac{a_5}{4} T^4 + a_7. \quad (3)$$

These parameters can be interactively calculated on the QDB website for specified temperatures (in K) with user specified other units such as eV, J, eV mol⁻¹, J mol⁻¹ for the enthalpy of formation. The NASA polynomials themselves are also available from the website. We are currently using modern compilations of partition functions [20–23] to compute new and updated NASA polynomials.

The Lennard-Jones parameters σ_{LJ} (LJS) and ϵ_{LJ} (LJE) as used in the intermolecular Lennard-Jones potential

$$V_{LJ}(r) = 4\epsilon_{LJ} \left[\left(\frac{\sigma_{LJ}}{r} \right)^{12} - \left(\frac{\sigma_{LJ}}{r} \right)^6 \right] \quad (4)$$

were added where available. These parameters were provided by references [24, 25] and Mark Kushner (private communication).

Experimental values for the spherical component of the polarisabilities, α_0 , are taken from the NIST Computational Chemistry Comparison and Benchmark Database (CCCBDB) [26]. Experimental values for the ionisation potentials, IP, which is the minimum energy required to remove an electron from the species, were taken from NIST Standard Reference Database 69: NIST Chemistry WebBook. Where possible ionization potentials for excited states were added as the difference of the ionization potential of the ground state and the energy of the excited state.

It should be noted that not all data are available for all species. In particular, so far we only have a rather limited set

Table 2. Classification of processes considered in QDB.

Abbrev	Type of reaction	Description	Total
Electron processes			
EDX	Deexcitation	$e + A^* \rightarrow e + A$	2648
EEL	Elastic scattering	$e + A \rightarrow e + A$	554
EIN	Ionization	$e + A \rightarrow e + A^+ + e$	329
EIP	Ion pair creation	$e + AB \rightarrow A^+ + B^- + e$	3
EMT	Momentum transfer		20
ERR	Radiative recombination	$e + A^+ \rightarrow A + h\nu$	2
EDR	Dissociative recombination	$e + AB^+ \rightarrow A + B$	826
EDS	Dissociation	$e + AB \rightarrow e + A + B$	660
EDA	Dissociative attachment	$e + AB \rightarrow A + B^-$	153
EDE	Dissociative excitation	$e + AB \rightarrow A^* + B + e$	4
EDI	Dissociative ionization	$e + AB \rightarrow A^+ + B + 2e$	400
EEX	Electron-impact electronic excitation	$e + A \rightarrow e + A^*$	2228
ECX	Change of excitation	$e + A^* \rightarrow e + A^{**}$	9601
ERC	Recombination (general)	$e + A^{+z} \rightarrow A^{+(z-1)}$	41
EDT	Electron attachment	$e + A + B \rightarrow A + B^-$	50
EVX	Electron-impact vibrational excitation	$e + A \rightarrow e + A [v = *]$	615
EXR	Electron-impact rotational excitation	$e + A \rightarrow e + A [J = *]$	11
ETS	Electron total scattering	$e + A \rightarrow e + \Sigma A$	11
ETI	Electron total ionisation	$e + A \rightarrow e + e + \Sigma A^+$	15
ETA	Electron total attachment	$e + A \rightarrow \Sigma A^-$	8
ETD	Electron total dissociation	$e + A \rightarrow e + \Sigma A$	36
ETN	Electron total neutral dissociation	$e + A \rightarrow e + \Sigma A$	4
Heavy particle reactions			
HGN	Associative electron detachment	$A^- + B \rightarrow AB + e$	162
HCX	Charge transfer	$A^+ + B \rightarrow A + B^+$	3393
HIR	Heavy-particle interchange	$A + BC \rightarrow AB + C$	2805
HAC	Association	$A + B \rightarrow AB$	291
HIN	Heavy-particle collisional ionization	$A + B \rightarrow A + B^+ + e$	9
HIA	Heavy-particle associative ionization	$A + B \rightarrow AB^+ + e$	7
HPN	Penning ionization	$A + B^* \rightarrow A^+ + B + e$	49
HNE	Neutralization	$e + B^- \rightarrow B + 2e$	5
HMN	Ions recombination	$A^- + B^+ \rightarrow A + B$	1727
HDS	Heavy-particle collisional dissociation	$AB + C \rightarrow A + B + C$	169
HDX	Heavy-particle collisional deexcitation	$A + B^* \rightarrow A + B$	174
HDN	Heavy-particle dissociative neutralization	$AB^- + C^+ \rightarrow A + B + C$	1182
HDC	Heavy-particle dissociation and charge transfer	$AB + C^+ \rightarrow A^+ + B + C$	356
HDI	Heavy-particle dissociation and ionization	$AB + C^* \rightarrow A^+ + B + C$	6
HEX	Heavy-particle excitation	$A + B \rightarrow A + B^*$	155
HDT	Heavy-particle electron detachment	$A^- + B \rightarrow A + B + e$	53
HET	Heavy-particle electron transfer	$A^- + B \rightarrow A + B^-$	4
HFR	Heavy particle fragmentation	$AB \rightarrow A + B^*$	6
HRA	Heavy particle radiative association	$A + B \rightarrow AB + h\nu$	133
Photon processes			
PRD	Radiative-decay	$A^* \rightarrow A + h\nu$	10

of species-specific Lennard-Jones parameters. The entries will be added to as the appropriate data are identified.

2.3. Reactions

The second major data type in QDB is reactions. Here the word reactions is used as a generic name for all processes in which species interact with each other resulting in either changes in the species, e.g. through a chemical reaction, or of energy state, e.g. through electron impact excitation. QDB designates all the various processes that constitute a reaction using a three letter classification; table 2 summarises these classifications.

Note that a few of the classifications have been changed to align with the standard classification scheme proposed by the International Atomic Energy Agency [27]. Each reaction also contains a reference to the data source.

2.4. Surface processes

Apart from gas phase processes, a framework for surface processes was constructed for QDB. Surface processes are split into two categories:

- Processes described by a single coefficient used in plasma simulations such as sticking coefficients;

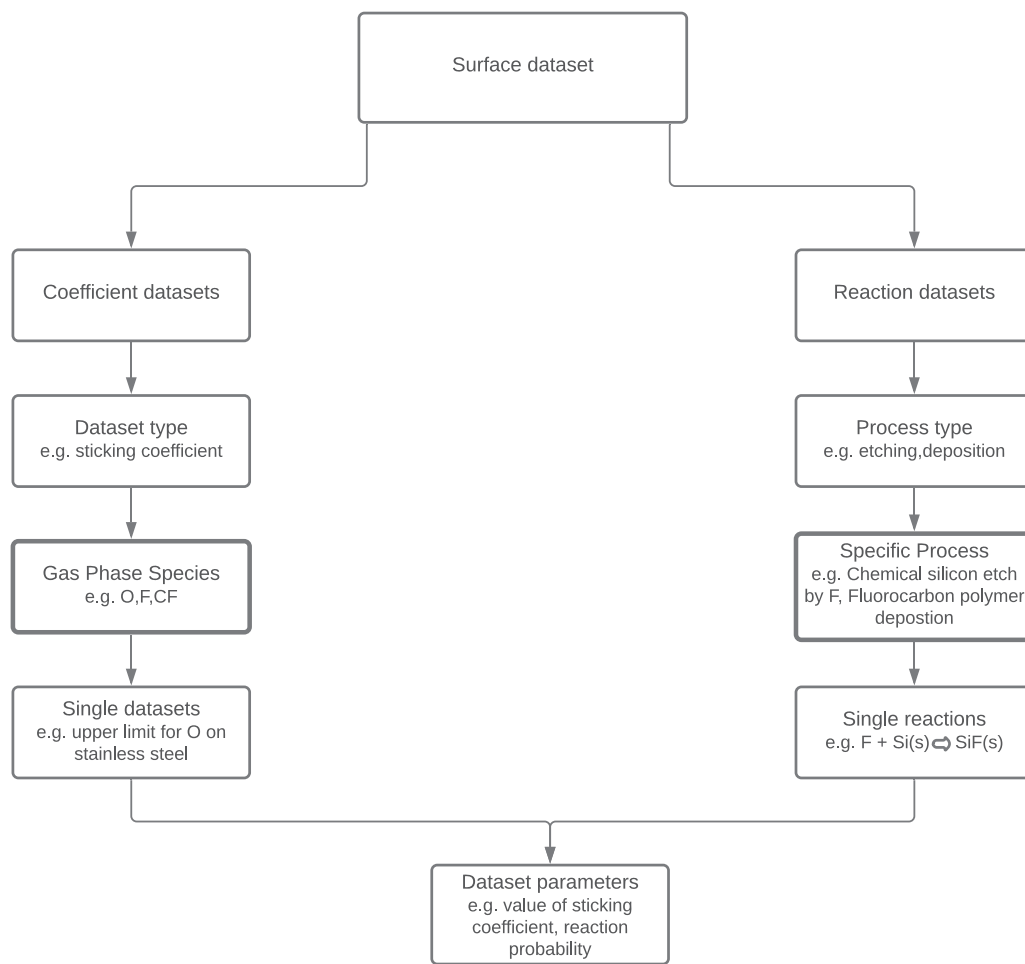


Figure 1. Hierarchical structure for storing and accessing data on surface processes. The data are presented to the user as collections of individual datasets, indicated by the bolder borders.

- Surface reactions used in surface simulations such as site-based models or feature profile simulation.

The single-coefficient processes datasets comprise simply the respective gas phase species (such as O), the surface involved (such as stainless steel), and the coefficient. Since these coefficients are not universal but depend on the process parameters such as power or pressure, usually a range of possible values is given rather than one definitive value. Sticking coefficients have been taken from references [28–36].

Surface reaction datasets comprise the gas phase species involved and surface species (which follow a similar database structure as the gas phase species) and the, in case of ion-induced processes optionally energy-dependent, coefficient. The data for such reactions are taken from articles describing site-based models [37, 38] or feature profile models [39–41] or both [42], which successfully recreated experimental results. As such, the individual surface reactions on their own do not carry useful information; they only have meaning as part of the entire mechanism. Hence, the individual reactions are grouped into sets of reactions and only these are accessible by the user. Essentially, the database gives access not to individual reactions but to sets of reactions describing a specific etching

or deposition process as a whole. The structure of the surface process data is visualized in figure 1.

It should be noted that data on surface processes usually has much larger uncertainties than, for example, electron collision cross sections. Thus, the QDB surface process data should rather be seen as guide lines, not as definitive data.

Although not completely included in the QDB database yet, energy and angle dependent sputtering yield data play an essential role in determining the profile evolution of surface features during etching and deposition processes, especially corner erosion and redeposition of sputtered or desorbed species from the surfaces of micro/nano-structures [41, 43, 44]. Indeed many experimentally measured sputtering yields as functions of the ion incident energy and angle of incidence have been published and some have been compiled in, e.g., references [45–47]. Most such data are for high-energy (> keV) ion incident energy and single-element ions. For semiconductor plasma processing applications, where low-energy ions are often used to avoid surface damages and incident ions are typically molecular fragments, rather than single-element ions, more data are needed. Yamamura and Tawara derived an empirical formula for the sputtering yields of single-element materials by single-element ions [46], which is available online [48]. Based on the experimental data summarized in reference

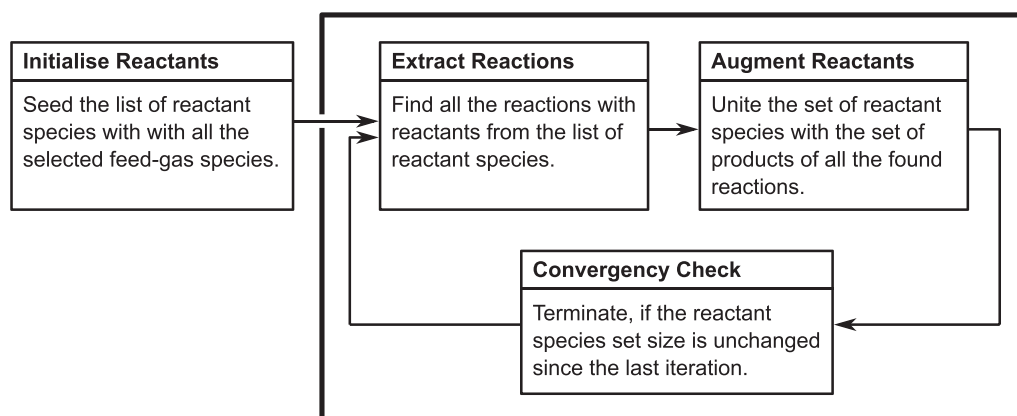


Figure 2. Schematic flow diagram of the chemistry generator algorithm.

[45], sputtering yields predicted by machine learning [49] are also available online [50].

2.5. Chemistry generator

While several pre-assembled and validated chemistry sets are available in QDB, they cover only a small fraction of possible plasma modeling applications. As the assembling of application-targeted chemistry sets is a crucial part of any plasma modeling workflow, a *Chemistry Generator* application was added to the QDB ecosystem to assist with this task. The chemistry generator simply takes the user input in the form of a set of selected feed-stock gases, and traverses the full collisional cascade of species and processes present in QDB. Figure 2 shows a schematic representation of the chemistry generator algorithm.

However, such approach can, if left unmediated, result in a very large number of species and reactions, especially in cases when one or more fragments or products of the feed-gas species has a large number of excited states present in the database. For that reason, users are additionally required to manually select the species of the full QDB reaction network, and their reactions. Species and reactions found in the full reaction network are clustered into several classes, while user has the ability to select all the species/reactions in any given class. Figure 3 shows the screenshot of the chemistry generator GUI in action.

As mentioned above, intervention from the user is currently required in the form of manually selecting individual species and reactions, or their groups. Without such user input, while including all the species and reactions found in the collisional cascade, the chemistry set built will include many redundant species and reactions, making it impractical for plasma modeling applications. In fact, almost all published chemistry sets contain redundant species and reactions [51]. The redundant species and reactions can be eliminated by various chemistry reduction techniques (CRT). Several review papers have dealt with the problem of chemistry reduction [52–56]. While these methods were traditionally mostly used by the combustion modeling community, some examples of CRT in plasma modeling applications can be found in the literature [57, 58]. A suitable automatic CRT was also lately

developed by Hanicinec *et al* [59]. We aim to integrate this method into the QDB chemistry generator workflow in the future, making the selection of required species and reactions fully automated, based on user inputs of plasma modeling parameters and conditions.

2.6. Boltzmann solver

A Boltzmann-solver was developed and integrated into the QDB environment to calculate electron energy distribution functions (EEDF) using the cross-sectional data in QDB. This solver is based on the Rockwood formalism [60]. The major difference between the original formalism and the one implemented in QDB is the use of a non-uniform energy grid in the QDB solver. This allows the resolution of fine structures in both cross sections and EEDFs as well as small energy losses (e.g. due to vibrational excitation) in the low-energy range. At higher energies, both cross sections and EEDFs typically show less structures and small energy inelastic collisions are negligible compared to high energy processes such as ionization. Incrementally increasing the energy interval therefore reduces the computational load without reducing the accuracy. For ionization, the colliding electron's energy is reduced by the ionization energy and a new electron is added to the lowest energy bin. For attachment/recombination, the colliding electron is completely removed. Since this changes the number of total electrons in the EEDF, it is renormalized after reaching convergence before calculating rates.

Within the QDB environment, the Boltzmann-solver can be applied to both pre-assembled sets and sets constructed with the chemistry generator. The solver uses all cross-sectional data included in a pre-assembled set or selected by the user in the generator. The user sets the relative densities of the heavy particles and the gas temperature (for the energy transfer by elastic collisions). The Boltzmann-solver is run for several values of the reduced electric field E/N and outputs.

- The EEDFs for the different E/N values
- The effective electron temperature as function of E/N
- The rate coefficients for the used electron collision processes as function of the effective electron temperature.

REACTION SELECTION AND DOWNLOADS
BOLTZMANN SOLVER
GLOBAL MODEL

FEED GASES

SPECIES

REACTIONS

CHARGE EXCHANGE - 10 REACTIONS

ELECTRON IMPACT RECOMBINATION - 7 REACTIONS

NEUTRAL CONVERSION - 19 REACTIONS

HEAVY PARTICLE DE-EXCITATION - 2 REACTIONS

ELECTRON IMPACT DISSOCIATION - 1 REACTIONS

ELECTRON IMPACT IONIZATION - 4 REACTIONS

Select All

$e^- + Ar \rightarrow e^- + e^- + Ar^+$
 $e^- + O_2 \rightarrow e^- + e^- + O_2^+$
 $e^- + O_2 \rightarrow e^- + e^- + O^+ + O$
 $e^- + O \rightarrow e^- + e^- + O^+$

ELECTRON ELASTIC COLLISIONS - 5 REACTIONS

ELECTRON MOMENTUM TRANSFER - 2 REACTIONS

Download Formats

You have downloaded 0 of 20 dynamic chemistry sets in the last 30 days.

Please select a file format.

HPEM
 CHEMKIN
 VizGlow
 COMSOL
 CFD-ACE
 References

UPDATE

DOWNLOAD

SAVE CHEMISTRY SET

Figure 3. Chemistry generator GUI example. In the first step (not depicted), O₂ and Ar feed gases were selected. In the second step (not depicted), only species O, O₂, O₃, Ar, O⁺, O₂⁺ and Ar⁺ were selected, ignoring all the other ions and all the excited species present in QDB. In the third step (depicted), the specific processes are selected, grouped into classes. Once the selection is complete, the chemistry can be downloaded in one of the supported formats, or saved for future reference.

The data is displayed as graphs in the website and can be downloaded in text format.

2.7. Zero-dimensional model

The *Quantemol global model (QGM)* has been developed and implemented to the QDB ecosystem, to allow users running fast calculations with both pre-assembled chemistry sets, and dynamically generated chemistry sets (section 2.5). QGM is built around the PyGMol (Python global model) backend, developed by Hanicinec *et al* for automatic reduction of chemistry sets [59]. It should be noted that the model is approximate, and is more suited for investigating trends and gaining insight into chemistry sets, rather than for quantitative analysis. QGM is outlined in this section, while appendix A provides a full description of the model with all equations.

The model solves for the set of ordinary differential equations (ODE) consisting of the number density balance equation for each heavy species in the chemistry, in addition to the electron energy density balance equation. The particle density balance equation includes contributions from volumetric reactions, flow, and from diffusion losses (surface sinks) as well as surface sources. The electron energy density balance includes contributions of power from any external sources absorbed by the plasma, elastic and inelastic collisions between electrons and heavy species, generation and loss of electrons in volumetric reactions and power lost by electrons and ions surface losses.

The outputs of the model are the number densities of all the heavy species n_i , number density of electrons n_e and the electron temperature T_e . The user inputs to the model are plasma parameters, such as power, pressure, feed gas

flow rates, dimensions of the plasma and gas temperature. It should be noted that the electron density is not explicitly resolved, but arises from enforcing the charge neutrality. Also, the heavy species temperatures are not resolved by the model, but rather treated as a constant input parameter. Finally, although QDB supports cross-sectional data-sets and has its own Boltzmann solver (section 2.6), the collisional kinetics are parametrized in QGM using the Modified Arrhenius formula, see equations (A.3) and (A.4) in appendix A, which is, in case of the cross-sectional datasets, fitted on a grid of Maxwellian temperatures.

2.8. Data access and data formats

The data stored in the database is accessible directly via the website, an API, or downloads. Chemistry sets can be downloaded in various formats for plasma simulation packages:

- HPEM [61]: pre-assembled chemistry sets are available via the API, which gives the reactions in HPEM format ready to be copied into the chemistry input file. Dynamic sets can be directly downloaded as an input file. In both cases, some manual corrections might be necessary to make the input compatible with HPEM's internal species and cross-section library.
- QVT: pre-assembled chemistry sets can be directly imported into Quantemol's HPEM based QVT software via an API. Incompatible species and reactions are automatically converted or filtered out, so no manual adjustments need to be made. The API also provides a search for single reactions which can be added to chemistry sets and access to the chemistry generator via the QVT GUI. As with pre-assembled sets, reactions incompatible with HPEM's internal libraries are converted or filtered out automatically.
- COMSOL [62]: an archive with files can be downloaded. This includes a file with the cross sections used in the set and a file with species, both directly importable. Reactions using Arrhenius-coefficient are provided in a separate file and need to be added manually.
- CHEMKIN [63]: ready-to-use input files can be downloaded for both pre-assembled and dynamically created sets.
- CFD-ACE+ [64]: ready-to-use input files can be downloaded for both pre-assembled and dynamically created sets.
- VizGlow [65]: an archive containing a species and a reaction input file which can be directly imported can be downloaded.

Additionally, a file listing the references for all reactions used in a set is available for download in all cases.

Apart from reaction data, the results of the Boltzmann-solver and the global model can be downloaded. In case of the Boltzmann-solver, this is a file listing the effective electron temperature and the rate coefficients for each reaction used for each value of the reduced electric field. For the global model, the download includes a file listing the process parameters and final densities as well as the electron temperature, a list of all

reactions used with their Arrhenius parameters, and a .csv file with the transient densities and electron temperature.

The global model is also available as a separate desktop application which downloads the species and reaction data from the QDB website via an API. Constructing chemistry sets and running the model, however, is executed on the local computer.

3. New data

The data available via QDB are constantly being expanded. Below we describe the major extra datasets that have been added since the original release. Data on many individual processes have also been added. We welcome the submission of suitable data for inclusion in QDB.

3.1. Electron collisions with heavy noble gases

Electron collisions with Ne, Ar, Kr, and Xe atoms are a challenging problem, due to the splitting of the $(np^5)^2P_{3/2,1/2}$ ionic core and the strong term dependence of the valence orbitals in the $(np^5)n'\ell$ excited states. In recent years, the B-spline R-matrix (BSR) method (a close-coupling approach) that may utilize non-orthogonal sets of one-electron orbitals has been very successful to address these issues, since it allows the use of individually optimized term-dependent orbitals sets. A general computer code for non-relativistic and semi-relativistic (Breit–Pauli) BSR was published by Zatsarinny [66], and the method was later extended to a full-relativistic (Dirac–Coulomb) scheme [67]. An overview of the method with a list of applications until 2013 can be found in the Topical Review by Zatsarinny and Bartschat [68]. Updated versions of the BSR and DBSR codes are freely available and can be downloaded from Zatsarinny's GitHub site [69]. Examples using an already compiled and fully installed BSR code can be found on the Atomic, Molecular and Optical Sciences Gateway [70].

When combined with the R-matrix with pseudo-states (RMPS) approach [71], in which a large number of (discrete) states are squeezed into the R-matrix box and then included in the close-coupling expansion, it is possible to account for the effect of coupling to both the high-lying Rydberg states and the ionization continuum on the cross sections for electron-induced transitions between the low-lying physical bound states. Furthermore, excitation of the positive-energy pseudo-states provides a very good estimate of the ionization cross section. A major advantage of the approach is the consistency associated with a single unitary theory (close-coupling) in which all the results are extracted from the same model.

Using the BSR and DBSR codes, extensive databases have been created for electron collisions with Ne, Ar, Kr, and Xe; these databases have been added to QDB in their entirety. For e-Ne, radiative data [72] as well as cross sections from semi-relativistic [73] and non-relativistic RMPS [74] are available. For e-Ar, radiative data can be found in [75], and the most recent extensive calculation for electron-induced transitions included 500 states in the semi-relativistic model [73]. Finally,

for e-Kr and e-Xe, we have full-relativistic results from 69-state (Kr) [76] and 75-state (Xe) [77] models. In the latter calculations, only physical discrete states were coupled.

3.2. Electron collisions with helium

The electron-He collision problem has been treated very successfully by a number of close-coupling with pseudo-states approaches already a long time ago (see, for example, references [78–80]). The previous version of the QDB database contained comparatively old (though likely still reliable) data. Nevertheless, we now include new data based on the 498-state non-relativistic BSR-calculation carried out more recently by Zatsarinny and Bartschat [81] in the context of energy- and angle-differential ionization processes. These data are for elastic scattering, excitation, and ionization from the $(1s^2)^1S$ ground state in the energy range from the respective thresholds up to 100 eV. Specifically, we include individual results for the lowest 11 states, i.e., up to $(1s3p)^1P^o$, then a sum over pseudo-states below the ionization threshold that is expected to be a good approximation for the combined excitation of the infinite number of discrete Rydberg states, and finally a sum over the remaining pseudo-states that approximates the true ionization cross section. The steps in the energy grid are relatively narrow, but still too coarse to resolve all but the most important resonances just below the first excited level and the ionization threshold. However, the data provided should be sufficient for plasma modelling, where such details are generally not required.

3.3. Reaction data from UMIST and KIDA

Data on reactions from both the KIDA [5, 6] and the UMIST Database for Astrochemistry (UDfA) [82] were added to QDB. Both databases mostly contain heavy particle reactions in form of ion–ion recombination, charge exchange, and various neutral–neutral reactions with some electron collisions, mostly recombination. The databases cover a large range of neutral species as well as positive and negative ions; the focus for both is on astrochemistry, so these species are mostly C and H containing molecules and include some N, O, S, P, and Si containing species as well; there are also few cases of molecules containing F, Fe, Cl, Mg or He.

Both databases were automatically parsed and compared to data already in QDB; missing reactions, species, rate coefficients, and original sources were then added. The KIDA database also contains some evaluation of the reaction data; only rate coefficients evaluated as recommended were added. Adding reactions from these databases led to the addition of three new reaction classifications; heavy-particle electron transfer (HET in table 2), heavy-particle fragmentation (HFR), and heavy-particle radiative association (HRA). It should be noted that both databases also contain rate coefficients in expressions other than the Arrhenius form; since QDB currently does not support these formats, these data were not added to QDB for the time being.

3.4. Electron collisions with iodine

Iodine is being considered as potential fuel for electric propulsion applications in which ionized gas is electrostatically accelerated to generate thrust. This form of thrust generation can significantly increase the payload-to-spacecraft mass ratio as compared to conventional chemical propulsion [83]. The potential use of iodine Hall-effect thrusters [84], in which electrons emitted from a cathode spiral around the thruster axis due to the combination of an axial electric and a radial magnetic field [83, 85], has led to a demand for data on electron collisions with both atomic and molecular iodine. Very recently Ambalampitiya *et al* [86] published a series of e – I_2 scattering cross sections computed using R-matrix procedures. These cross sections have now been added to QDB.

3.5. Vibrationally resolved reactions involving N_2 and O_2

Very extensive datasets of vibrationally-resolved processes involving molecular nitrogen and molecular oxygen have been added to the database. These reactions, which are important for models of atmospheric plasmas, are described in section 4.4 below.

4. Use cases

4.1. Comparison between QGM and LoKI

QGM results were compared against another global model solver, the LisOn kinetics (LoKI), for the pre-assembled chemistry of oxygen, available at QDB. The analysis adopted two sets of working conditions, considering different gas pressures and electron densities. The following sections present a brief description of the LoKI simulation tool, highlighting differences with respect to QGM and some modifications introduced for the comparison, a summary of the data and working conditions adopted in the simulations, and a discussion of the results obtained.

4.1.1. The LoKI simulation tool. LoKI [87] is a simulation tool developed under MATLAB, that couples two main calculation blocks: (i) a Boltzmann solver (LoKI-B) for the electron Boltzmann equation, released as open-source code licensed under the GNU general public license [88, 89], and (ii) a chemical solver (LoKI-C) for the global kinetic model(s) of pure gases or gaseous mixtures, which solves the zero-dimensional (volume average) number density balance equation for each heavy species in the plasma chemistry. In this workflow, and in contrast to QGM, the balance of the electron energy–density is described by the (homogeneous) electron Boltzmann equation, thus including contributions only due to the power gained/lost from external sources to the plasma and from collisions (elastic, inelastic, superelastic, and non-conservative volumetric reactions). On the other hand, the particle balance equations can include contributions similar to

QGM: volumetric reactions, flow and transport mechanisms, including interaction with the surfaces. LoKI includes also a thermal model for the heavy-species, to self-consistently calculate the gas temperature.

LoKI receives the input data via two intuitive parser-files: a setup file defining the physical and numerical working conditions, and a chemistry file detailing the kinetic scheme and data adopted. The latter file was easily constructed for the pre-assembled chemistry of QDB, which involved (i) electron-impact reactions and heavy-species collisions, both described using Arrhenius-type or power-law rate coefficients (depending on the electron temperature or the gas temperature); and (ii) transport + wall-recombination models, for both charged and neutrals species.

Since electron-impact reactions are described here by imposing T_e -dependent rate coefficients, there is no need to calculate a non-equilibrium EEDF, hence LoKI-C was used as standalone tool without a coupling to LoKI-B. In this case, and for given plasma parameters (e.g. gas pressure and temperature, electron density, dimensions of the plasma), the code evaluates the densities of the various charged/neutral heavy-species in an iterative procedure that changes the electron temperature (hence the densities of the ions) so as to satisfy the neutrality condition.

LoKI's workflow further includes a *pressure cycle* where the initial composition of the gas mixture is adjusted to ensure that dissociation/association and wall-interaction mechanisms lead to a final gas pressure equal to the working pressure. In QGM, the *pressure regulation* adopts a different strategy, by including an additional outflow term in the balance equations of neutral species (see appendix A).

The major differences between LoKI and QGM are related to the physical models adopted for transport and wall-recombination. For positive ions, number density n_+ , LoKI describes the rate of wall-losses using

$$\left(\frac{\delta n_+}{\delta t}\right)_{\text{diff}}^{\text{out}} = -\frac{D_{\text{eff}+}}{\Lambda^2} n_+, \quad (5)$$

where Λ is the same effective diffusion length defined in (A.14) and $D_{\text{eff}+}$ is an effective ambipolar diffusion coefficient, obtained according to the formulation proposed in [90], for charged-particle transport in the presence of several positive ions and a single negative ion with low density. Numerical tests using this model showed considerable deviations between LoKI and QGM results, including different T_e -values by more than a factor of 2. For this reason, and also due to the limitations of LoKI's model with respect to negative ions, we have implemented in LoKI the QGM diffusion model for positive ions [91], described in appendix A.

In LoKI, the transport of neutral species i , number density n_i , adopts a model similar to that of QGM, with gain/loss rates given by

$$\left(\frac{\delta n_i}{\delta t}\right)_{\text{diff}} = \sum_j a_{ij}^R r_{ij} \frac{n_j}{\tau_j} - \frac{n_i}{\tau_i}, \quad (6)$$

with τ_i the characteristic transport time due to the combined effect of diffusion and recombination at the wall

$$\tau_i = \frac{\Lambda^2}{D_i} + 4 \frac{1 - s_i/2}{s_i \bar{v}_i} \frac{V}{A}, \quad (7)$$

where D_i are multi-component diffusion coefficients calculated adopting Wilke's model [92] and where the total sticking coefficient is identified with a wall-loss probability of recombination of species i , returning to the volume as species k ($s_i = \sum_k \gamma_{ik}$). Note that equations (6) and (7) correspond to equations (A.12) and (A.13), if Λ is identified with V/A in the first term of (7) and if $s_i/2$ is neglected in the second term of (7). Here, the transport of neutral species was described adopting either the expressions presented above (simulations labeled *LoKI original*) or neglecting the diffusion transport for atomic species using adjusted wall-loss probabilities (simulations labeled *LoKI modified*), taking

$$\tau_{\text{wall}_i} \simeq 4 \frac{1 - s_i/2}{s_i \bar{v}_i} \frac{V}{A}. \quad (8)$$

4.1.2. Kinetic scheme and data. Working conditions. QGM and LoKI were compared for the pre-assembled oxygen chemistry available from QDB. Table 3 summarizes the kinetic scheme and data adopted in the simulations, which involve the molecular species $\text{O}_2(\text{X}, v = 0-6)$, $\text{O}_2(\text{a}^1\Delta_g)$, O_2^+ , O_2^- , $\text{O}_3(\text{X})$ and O_3^- ; and the atomic species $\text{O}(\text{^3P})$, $\text{O}(\text{^1D})$, O^+ and O^- .

In table 3, the wall-loss probabilities for ions and for molecular neutral species were taken equal to 1, whereas for atomic neutral species they were either also taken equal to 1 (*LoKI original*) or adjusted according to the working conditions (*LoKI modified*).

The simulations considered two sets of working conditions: a high-pressure scenario at $p = 10^4$ Pa and $n_e = 2 \times 10^{14} \text{ m}^{-3}$, for which the atomic wall-recombination probabilities were set to $s_{\text{O}} = 7 \times 10^{-4}$ and $s_{\text{O}^*} = 5 \times 10^{-4}$; a low-pressure scenario at $p = 3$ Pa and $n_e = 10^{16} \text{ m}^{-3}$, with $s_{\text{O}} = 0.5$ and $s_{\text{O}^*} = 0.3$. In both cases, $T_g = 500$ K.

4.1.3. Results and discussion. Figures 4 and 5 present the densities of the different species considered in the model, for the high and low pressure conditions, respectively, calculated with QGM. For comparison, these figures show also the percent deviation with respect to LoKI results, adopting either the *LoKI original* or the *LoKI modified* configurations (see section 4.1.1). In both high/low pressure cases, the plasma is dominated by the vibrational ground-state $\text{O}_2(\text{X}, v = 0)$, exhibiting a low degree of dissociation ($\sim 4 \times 10^{-2}\%$); the most abundant ion species are O_2^+ and O^- , with similar densities 3–35 times greater than n_e .

Figures 4 and 5 show a considerable decrease in the deviations between QGM and LoKI when using for the same kinetic scheme but with adjusted conditions for the transport of atomic neutral species (configuration *LoKI modified*). At high pressure, although the modifications in the transport model are directly aimed at changing the densities of $\text{O}(\text{^3P})$ and $\text{O}(\text{^1D})$, they have a global effect upon the gains/losses of all species, contributing to reduce the deviations between LoKI and QGM

Table 3. Summary of the oxygen kinetic scheme and data adopted in the simulations. T_e is in eV, T_g is in K, and the probabilities s are dimensionless.

Reaction	Rate coefficient (m^{-3})
Electron impact collisions	
$e + \text{O}_2(X, v = 0-1) \rightarrow e + 2\text{O}(^3\text{P})$	$1.73 \times 10^{-14} T_e^{-1.27} \exp(-7.33/T_e)$
$e + \text{O}_2(X, v = 1-6) \rightarrow e + \text{O}(^3\text{P}) + \text{O}(^1\text{D})$	$2.51 \times 10^{-14} T_e^{0.20} \exp(-6.44/T_e)$
$e + \text{O}_2(X, v = 0) \rightarrow e + \text{O}_2(a^1\Delta_g)$	$2.71 \times 10^{-15} T_e^{-0.32} \exp(-3.25/T_e)$
$e + \text{O}_2(X, v = 0) \rightarrow 2e + \text{O}_2^+$	$1.44 \times 10^{-14} T_e^{0.54} \exp(-15.51/T_e)$
$e + \text{O}_2(X, v = 0) \rightarrow 2e + \text{O}(^3\text{P}) + \text{O}^+$	$1.49 \times 10^{-15} T_e^{0.98} \exp(-21.25/T_e)$
$e + \text{O}_2(X, v = 0) \rightarrow e + \text{O}(^3\text{P}) + \text{O}^-$	$1.93 \times 10^{-15} T_e^{-1.23} \exp(-7.33/T_e)$
$e + \text{O}_2(a^1\Delta_g) \rightarrow 2e + \text{O}_2^+$	$1.30 \times 10^{-15} T_e^{1.10} \exp(-11.1/T_e)$
$e + \text{O}_2^+ \rightarrow e + 2\text{O}(^3\text{P})$	$1.53 \times 10^{-14} T_e^{-0.50} \exp(-0.02/T_e)$
$e + \text{O}(^3\text{P}) \rightarrow 2e + \text{O}^+$	$3.54 \times 10^{-15} T_e^{0.83} \exp(-12.21/T_e)$
$e + \text{O}(^1\text{D}) \rightarrow 2e + \text{O}^+$	$1.42 \times 10^{-14} T_e^{0.35} \exp(-13.23/T_e)$
$e + \text{O}^- \rightarrow 2e + 2\text{O}(^3\text{P})$	$1.95 \times 10^{-18} T_e^{-0.50} \exp(-3.40/T_e)$
$e + \text{O}_3(X) \rightarrow \text{O}_2(X, v = 0) + \text{O}^-$	$1.92 \times 10^{-15} T_e^{-1.31} \exp(-1.01/T_e)$
$e + \text{O}_3(X) \rightarrow \text{O}(^3\text{P}) + \text{O}_2^-$	$8.87 \times 10^{-16} T_e^{-1.42} \exp(-1.07/T_e)$
$e + \text{O}_2(X, v = 0) \rightarrow e + \text{O}_2(X, v = 1)$	$4.88 \times 10^{-16} T_e^{-1.42} \exp(-0.56/T_e)$
$e + \text{O}_2(X, v = 0) \rightarrow e + \text{O}_2(X, v = 2)$	$1.81 \times 10^{-16} T_e^{-1.45} \exp(-0.83/T_e)$
$e + \text{O}_2(X, v = 0) \rightarrow e + \text{O}_2(X, v = 3)$	$9.90 \times 10^{-15} T_e^{-1.14} \exp(-7.62/T_e)$
$e + \text{O}_2(X, v = 0) \rightarrow e + \text{O}_2(X, v = 4)$	$6.72 \times 10^{-15} T_e^{-1.23} \exp(-7.93/T_e)$
$e + \text{O}_2(X, v = 0) \rightarrow e + \text{O}_2(X, v = 5)$	$3.67 \times 10^{-14} T_e^{-1.12} \exp(-7.43/T_e)$
$e + \text{O}_2(X, v = 0) \rightarrow e + \text{O}_2(X, v = 6)$	$1.60 \times 10^{-14} T_e^{-1.11} \exp(-7.36/T_e)$
Heavy species collisions	
$2\text{O}_2(X, v = 0) \rightarrow \text{O}(^3\text{P}) + \text{O}_3(X)$	$1.11 \times 10^{-17} T_g^{-49800}$
$\text{O}_2(X, v = 0) + \text{O}_2(a^1\Delta_g) \rightarrow \text{O}(^3\text{P}) + \text{O}_3(X)$	2.95×10^{-27}
$\text{O}(^3\text{P}) + \text{O}_3(X) \rightarrow 2\text{O}_2(X, v = 0)$	$8.00 \times 10^{-18} \exp(-2060/T_g)$
$\text{O}_2(X, v = 0) + \text{O}^+ \rightarrow \text{O}(^3\text{P}) + \text{O}_2^+$	$1.96 \times 10^{-16} T_g^{-0.40}$
$\text{O}_2(X, v = 0) + \text{O}^- \rightarrow \text{O}(^3\text{P}) + \text{O}_2^-$	2.50×10^{-20}
$\text{O}_2(X, v = 0) + \text{O}^- \rightarrow e + \text{O}_3(X)$	5.00×10^{-21}
$\text{O}_2(X, v = 0) + \text{O}_2^- \rightarrow \text{O}(^3\text{P}) + \text{O}_3^-$	3.00×10^{-21}
$\text{O}_2(X, v = 0) + \text{O}_2^- \rightarrow e + 2\text{O}_2(X, v = 0)$	$1.56 \times 10^{-17} T_g^{0.50} \exp(-5590/T_g)$
$\text{O}(^3\text{P}) + \text{O}^- \rightarrow e + \text{O}_2(X, v = 0)$	$5.20 \times 10^{-15} T_g^{-0.50}$
$\text{O}(^3\text{P}) + \text{O}_2^- \rightarrow \text{O}_2(X, v = 0) + \text{O}^-$	3.30×10^{-16}
$\text{O}(^3\text{P}) + \text{O}_2^- \rightarrow e + \text{O}_3(X)$	1.50×10^{-16}
$\text{O}(^3\text{P}) + \text{O}_3^- \rightarrow \text{O}_2(X, v = 0) + \text{O}_2^-$	3.20×10^{-16}
$\text{O}(^3\text{P}) + \text{O}_3^- \rightarrow e + 2\text{O}_2(X, v = 0)$	3.00×10^{-16}
$\text{O}_3(X) + \text{O}^+ \rightarrow \text{O}_2(X, v = 0) + \text{O}_2^+$	1.00×10^{-16}
$\text{O}_3(X) + \text{O}^- \rightarrow \text{O}_2(X, v = 0) + \text{O}_2^-$	$5.89 \times 10^{-19} T_g^{0.50}$
$\text{O}_3(X) + \text{O}^- \rightarrow \text{O}(^3\text{P}) + \text{O}_3^-$	5.30×10^{-16}
$\text{O}_3(X) + \text{O}_2^- \rightarrow \text{O}_2(X, v = 0) + \text{O}_3^-$	4.00×10^{-16}
$\text{O}_2^+ + \text{O}^- \rightarrow \text{O}_2(X, v = 0) + \text{O}(^3\text{P})$	1.00×10^{-13}
$\text{O}_2^+ + \text{O}^- \rightarrow 3\text{O}(^3\text{P})$	$3.46 \times 10^{-12} T_g^{-0.50}$
$\text{O}_2^+ + \text{O}_2^- \rightarrow \text{O}_2(X, v = 0) + 2\text{O}(^3\text{P})$	1.00×10^{-13}
$\text{O}_2^+ + \text{O}_2^- \rightarrow 2\text{O}_2(X, v = 0)$	1.00×10^{-13}
$\text{O}_2^+ + \text{O}_3^- \rightarrow 2\text{O}(^3\text{P}) + \text{O}_3(X)$	1.00×10^{-13}
$\text{O}_2^+ + \text{O}_3^- \rightarrow \text{O}_2(X, v = 0) + \text{O}_3(X)$	1.00×10^{-13}
$\text{O}^+ + \text{O}^- \rightarrow 2\text{O}(^3\text{P})$	1.00×10^{-13}
$\text{O}^+ + \text{O}_2^- \rightarrow \text{O}_2(X, v = 0) + \text{O}(^3\text{P})$	1.00×10^{-13}
$\text{O}^+ + \text{O}_3^- \rightarrow \text{O}(^3\text{P}) + \text{O}_3(X)$	1.00×10^{-13}
$\text{O}^+ + \text{O}_3^- \rightarrow \text{O}_2(X, v = 0) + 2\text{O}(^3\text{P})$	1.00×10^{-13}
Transport of heavy species (see text)	
$\text{O}_2^+ + \text{wall} \rightarrow \text{O}_2(X, v = 0)$	s_+
$\text{O}^+ + \text{wall} \rightarrow \text{O}(^3\text{P})$	s_+
$\text{O}_2(a^1\Delta_g) + \text{wall} \rightarrow \text{O}_2(X, v = 0)$	s_{O_2}
$\text{O}_2(X, v = 1-6) + \text{wall} \rightarrow \text{O}_2(X, v = 0)$	s_{O_2}
$\text{O}(^3\text{P}) + \text{wall} \rightarrow (1/2)\text{O}_2(X, v = 0)$	s_{O}
$\text{O}(^1\text{D}) + \text{wall} \rightarrow \text{O}(^3\text{P})$	s_{O^*}

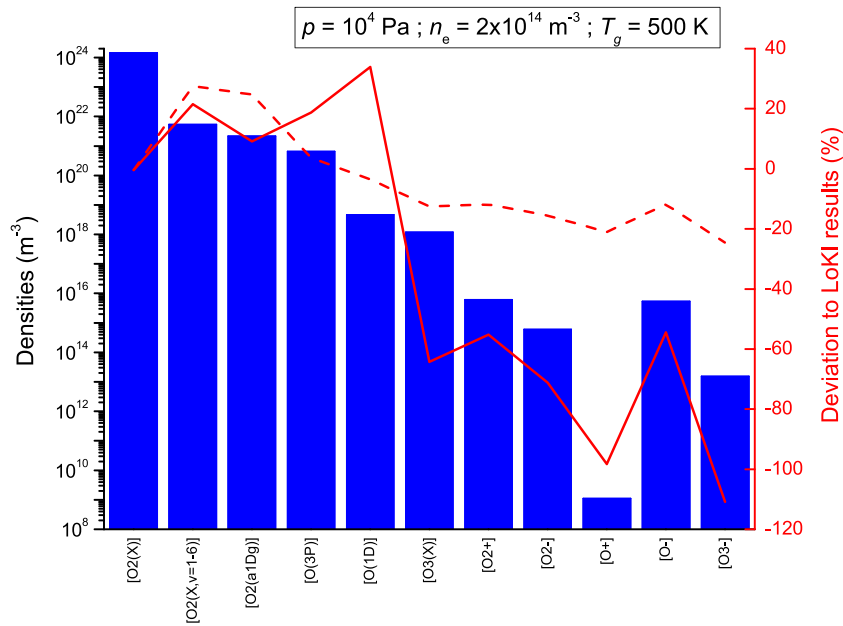


Figure 4. Density of oxygen species calculated with QGM at high-pressure (blue bars; left scale): $p = 10^4 \text{ Pa}$, $T_g = 500 \text{ K}$ and $n_e = 2 \times 10^{14} \text{ m}^{-3}$. Percent deviation of the results with respect to LoKI calculations (red curves; right scale), obtained adopting the code *LoKI original* (solid curve) or a *LoKI modified* version (dashed) with adjusted conditions for the wall-losses of $\text{O}(^3\text{P})$ and $\text{O}(^1\text{D})$. In this figure, $\text{O}_2(\text{X})$ is equivalent to $\text{O}_2(\text{X}, v = 0-6)$, including the full vibrational manifold of the electronic ground-state of molecular oxygen.

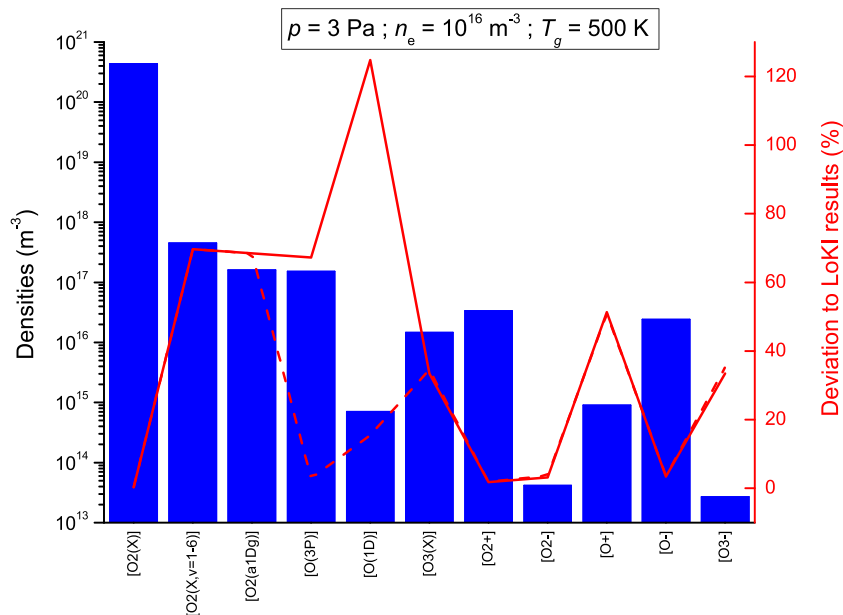


Figure 5. As in figure 4, but for low-pressure conditions: $p = 3 \text{ Pa}$, $T_g = 500 \text{ K}$ and $n_e = 10^{16} \text{ m}^{-3}$.

to values below 20%. The effect extends even to the calculated electron temperature ($T_e = 1.18 \text{ eV}$, as predicted by QGM), for which deviations of 8.6% and 1.7% are found with respect to *LoKI original* and *LoKI modified*, respectively.

At low pressure, electron-impact processes have an increased influence in the kinetic scheme, hence the differences in the calculated electron temperature (4% for both *original* and *modified* LoKI configurations, with respect to the QGM prediction of $T_e = 3.25 \text{ eV}$) are responsible for deviations in the density of species that are still between

$\sim 0.3\% - 70\%$, even for *LoKI modified*. In this case, the modifications in the transport model have an almost exclusive effect upon the densities of $\text{O}(^3\text{P})$ and $\text{O}(^1\text{D})$.

The previous analysis highlights the importance of transport models in the overall accounting of the gain/loss rates of species in a plasma. Note that the above agreement between QGM and LoKI was obtained after adopting the same transport model for charged-species, and after neglecting the diffusion transport for atomic species using adjusted wall-loss probabilities (see section 4.1.1).

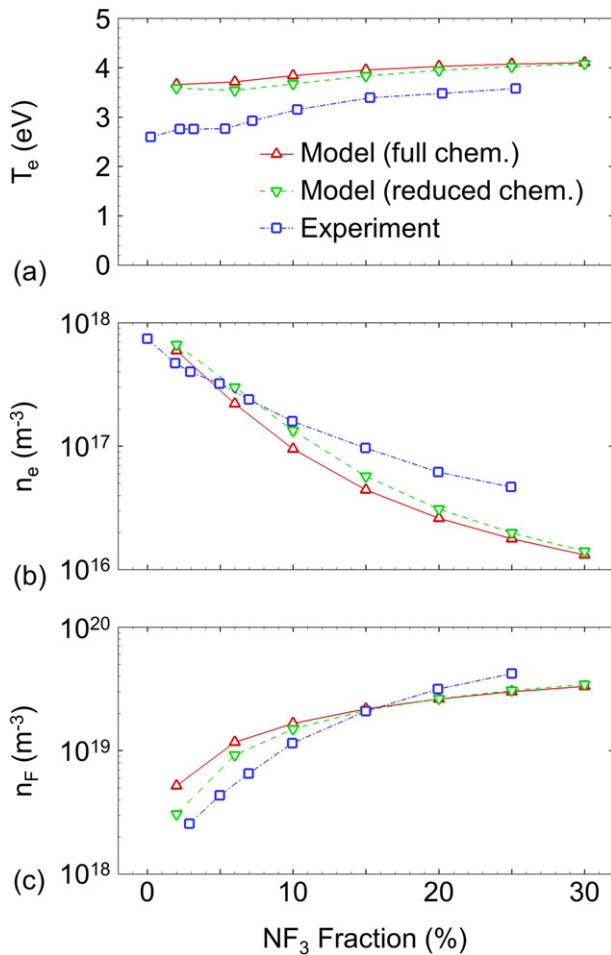


Figure 6. Effect of NF₃ fraction in Ar/NF₃ plasma on (a) electron temperature (T_e) 4.5 cm above the center of the bottom electrode, (b) electron density (n_e) 4.5 cm above the bottom electrode and (c) volume averaged F density. Modeling results obtained using the full and reduced chemistry have been compared to experimental results from Kimura and Hanaki [97]. The plasma power is 140 W in these results.

4.2. Modeling of inductively coupled Ar/NF₃/O₂ and Ar/NF₃ plasmas

Ar/NF₃/O₂ and Ar/NF₃ inductively coupled plasmas (ICP) have been modeled [38, 93] using the reaction set obtained from QDB, see reference [94]. The fluid and hybrid plasma model, CRTRS (see reference [95] and the citations therein), was used for this modeling project. Succinctly, for the results discussed in this paper, the simulations include a frequency-domain electromagnetic model of the ICP source coupled to an electrostatic model of the plasma. The plasma model includes the Poisson equation, continuity equation for all charged and neutral species, momentum equation for ions, and energy equation for electrons. The model considers gas flow using OpenFOAM [96], which is coupled to the plasma model. The Ar/NF₃/O₂ plasma chemical mechanism is described and used in references [38, 93] and includes 39 species and 308 reactions. The chemistry data (reactions and cross sections) from QDB were used in CRTRS with minor modifications. The Boltzmann equation was solved to compute the reaction rates for electron impact reactions and electron transport coefficient

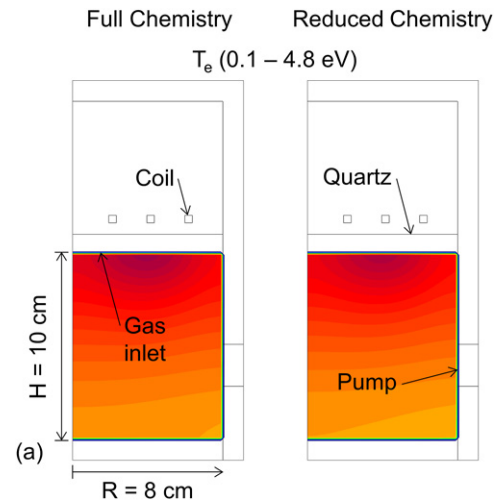


Figure 7. Electron temperature (T_e) using the full and reduced chemistries. These simulations have been done for an Ar/NF₃/O₂ = 80/10/10% plasma at 30 mTorr and 140 W plasma power.

(as a function of the electron temperature T_e) using the cross sections provided. The gas and ion temperatures were assumed to be 1000 K in the simulations. The F recombination coefficient ($F \rightarrow F_2$) was adjusted in the mechanism to 0.004 based on comparison with experimental results (discussed below).

After an initial set of simulations with the full chemistry, a reduced-order chemistry was also developed and simulated. The reduction method is described in detail in reference [59]. In short, the results of one simulation using a global plasma model for given process parameters with the full set is used to rank the species in the set with regards to their influence on the densities of species of interest, e.g. neutral radicals which induce the desired surface interactions. For the reduction itself, the species are then removed in reverse order, i.e. the lowest-ranking species first, and a test run of the global model to establish whether the densities of the specified species of interest stay within a set error margin compared to the full set. If so, the species is considered to be negligible and permanently removed from the set along with all its reactions; if not, the species is reinserted into the chemistry set. In this case, this reduction method was used using QGM for the process conditions detailed below with electrons and atomic F as species of interest to be preserved within 10%. To account for variations in the relative flows, the reduction was carried out independently for three cases (O₂ 5/10/15 sccm, NF₃ 15/10/5 sscm, Ar 80 sccm) and only species identified as negligible in all three cases were ultimately removed from the set for the 2D simulations. The reduced chemistry has 23 species and 100 reactions.

We next discuss the two-dimensional modeling of the ICP source described in reference [97]. Modeling was performed using both the full and reduced chemistries. One motivation for modeling this system was the extensive experimental data reported in reference [97]. Before the detailed modeling results are described, we focus on model validation and examine the effect of NF₃ fraction in Ar/NF₃ plasma on plasma properties. The results for (a) T_e 4.5 cm above the center of the bottom electrode, (b) electron density (n_e) 4.5 cm above

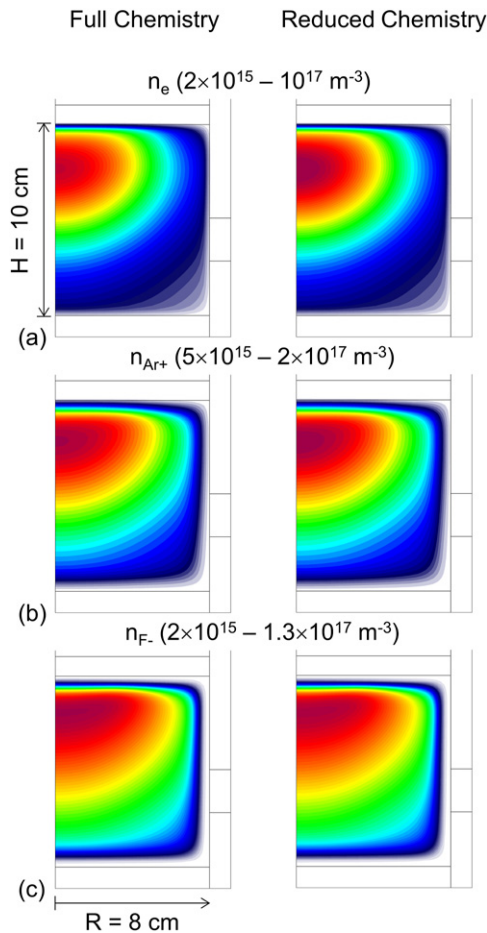


Figure 8. Density of (a) electrons (n_e), (b) Ar^+ ions (n_{Ar^+}) and (c) F^- ions (n_{F^-}) using the full and reduced chemistries. These simulations have been done for an $\text{Ar}/\text{NF}_3/\text{O}_2 = 80/10/10\%$ plasma at 30 mTorr and 140 W plasma power.

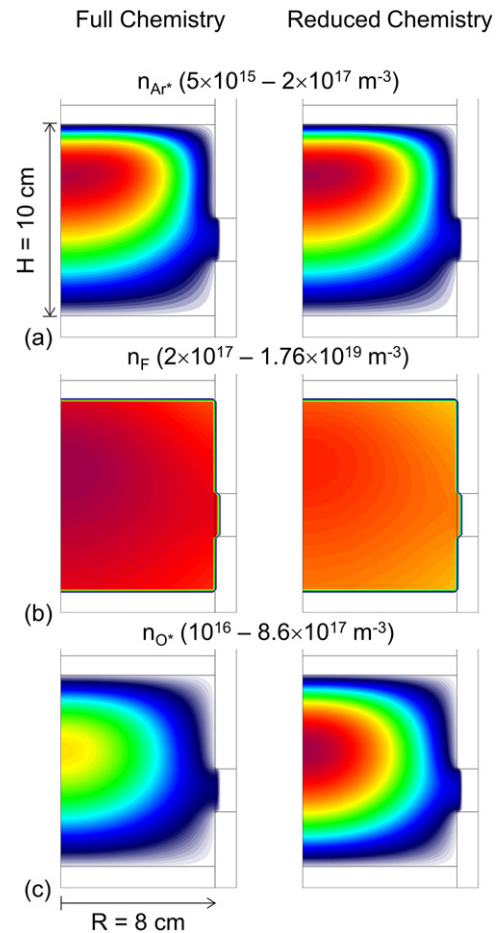


Figure 9. Density of (a) Ar^* (n_{Ar^*}), (b) F (n_{F}) and (c) O^* radicals (n_{O^*}) using the full and reduced chemistries. These simulations have been done for an $\text{Ar}/\text{NF}_3/\text{O}_2 = 80/10/10\%$ plasma at 30 mTorr and 140 W plasma power.

the bottom electrode, and (c) volume averaged F density are plotted in figure 6 as a function of NF_3 fraction. Modeling results obtained using the full and reduced chemistries have been compared to experimental data from reference [97]. The plasma power is 140 W and the gas pressure is 30 mTorr in these simulations and experiments. Results using both the full and reduced chemistries generally agree well with experimental measurements. T_e in the model is higher than the experiment, which is likely due to the use of the homogeneous Boltzmann equation for computing the EEDF and the reaction rates.

We next focus on a detailed comparison of modeling results from the simulations with full and reduced chemistries. The simulations in figures 7–9 were made for an $\text{Ar}/\text{NF}_3/\text{O}_2 = 80/10/10\%$ gas mixture at 30 mTorr pressure and 140 W plasma power. The gas mixture is assumed to be introduced uniformly below the quartz plate. T_e obtained using the full and reduced chemistries is shown in figure 7. T_e is highest below the quartz plate as ICP power is mostly coupled to electrons in this region. The densities of a few charged species (electrons, Ar^+ ions, and F^- ions) are compared in figure 8 using the full and reduced chemistries. Densities of these species peak at the center of the chamber due to diffusion. There is generally good

agreement between the full and reduced chemistry models. The overall chemistry is complex with many neutral species. We have compared the densities of a few important neutral radicals (Ar^* , F , O^*) in figure 9 using the full and reduced chemistries. Chemistry reduction was done to preserve F density, so F density is reasonably close between the two models. So is the density of Ar^* and many other neutral species (not shown). However, the O^* density highlights that not every quantity will be preserved with the reduced chemistry.

The comparison between models with full and reduced chemistries (in figures 7–9) was for one set of conditions. To understand better how well the chemistry reduction works, we have examined the effect of NF_3 fraction in $\text{Ar}/\text{NF}_3/\text{O}_2$ plasma on spatially averaged densities of electrons, Ar^+ ions, and F^- ions using the full and reduced chemistries in figure 10. Ar fraction is 80% in these simulations and O_2 fraction is 20%— NF_3 fraction. The simulations were made at 30 mTorr and 140 W plasma power. There is generally good agreement over the whole range of O_2/NF_3 gas mixture. Similarly, we look at the effect of NF_3 fraction in $\text{Ar}/\text{NF}_3/\text{O}_2$ plasma on spatially averaged densities of a few neutral species with the highest concentration (F, N_2 , O, and NF_2) in figure 11. There is generally good agreement between the full and reduced

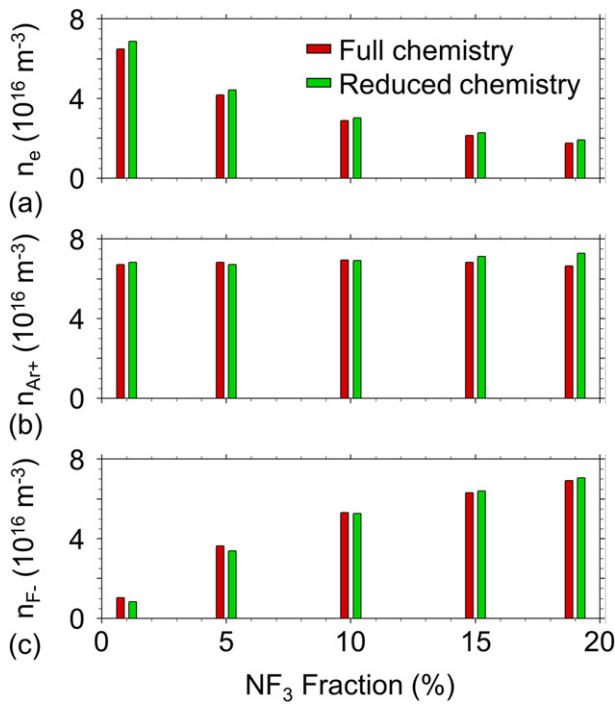


Figure 10. Effect of NF_3 fraction in $\text{Ar}/\text{NF}_3/\text{O}_2$ plasma on spatially averaged densities of (a) electrons (n_e), (b) Ar^+ ions (n_{Ar^+}) and (c) F^- ions (n_{F^-}) using the full and reduced chemistries. Ar fraction is 80% and O_2 fraction is 20%— NF_3 fraction. The simulations have been done at 30 mTorr and 140 W plasma power.

chemistries over the full range of O_2/NF_3 gas mixture, demonstrating the transferability of the reduction method using a global model to multi-dimensional models.

4.3. Modeling reactive species formation in $\text{He}/\text{H}_2\text{O}$ -based plasma jets at atmospheric pressure

This section illustrates a use case for the chemical reduction method described in reference [59], which is planned for future integration into QDB. In addition, some important aspects to be considered when carrying out reduction of plasma-chemical reaction sets are demonstrated. Here, the formation of reactive species in atmospheric pressure plasma sources, acts as a focus. In general, reactive species formation is of crucial importance for applications in biomedical and surface treatment. Accurate simulation of the absolute densities of these species is challenging due to the complex reaction pathways, which can involve a large number of production and consumption processes. Since the most important processes are often difficult to identify *a priori* a common approach is to start with a model containing a large number of species and reactions so as to minimise the likelihood of omitting important processes. The requirement to treat large numbers of species means that computationally efficient global models are typically used for such studies. These models allow for detailed insight into the chemical pathways, at the cost of a simplified treatment of the physical processes, such as electron heating. In order to develop simplified sets of chemical reactions for use with more complex physical models, the elimination of species and reactions using chemical reduction techniques is a promising

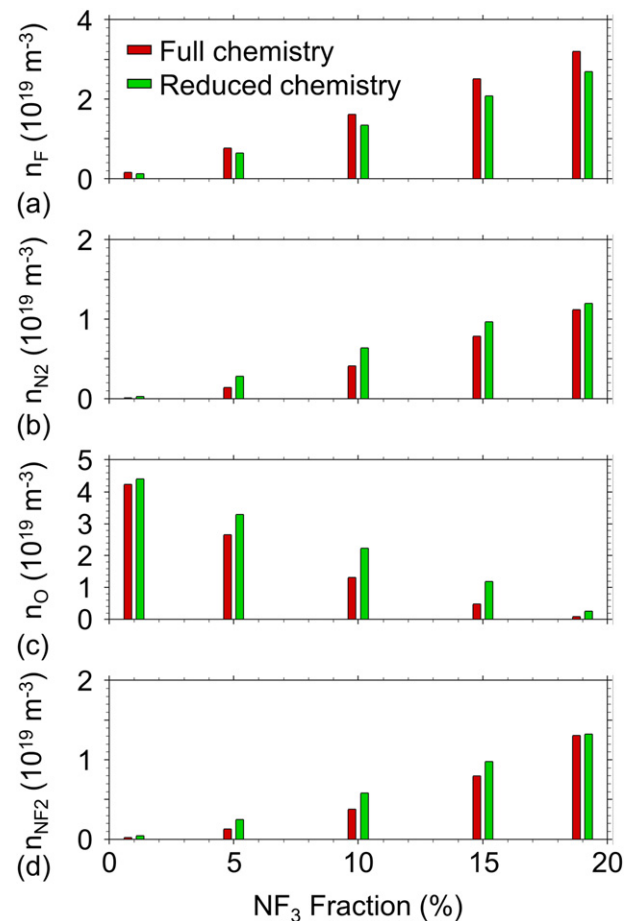


Figure 11. Effect of NF_3 fraction in $\text{Ar}/\text{NF}_3/\text{O}_2$ plasma on spatially averaged densities of (a) F (n_{F}), (b) N_2 (n_{N_2}), (c) O (n_{O}), and (d) NF_2 (n_{NF_2}) using the full and reduced chemistries. Ar fraction is 80% and O_2 fraction is 20%— NF_3 fraction. The simulations have been done at 30 mTorr and 140 W plasma power.

approach. However, any such reduction should be performed carefully in order to ensure that important pathways are not removed accidentally. In addition, the plasma parameter range over which the reduced reaction set (RRS) is valid should be clearly defined as pathways that are unimportant under a certain set of operating conditions may be essential under other operating conditions.

In this section, the chemical reduction method described in reference [59] is applied to the reaction set for $\text{He}/\text{H}_2\text{O}/\text{O}_2$ originally developed in reference [98] and extended in reference [99]. When used in the global model framework, GlobalKin, developed by Kushner and co-workers [100], this reaction mechanism leads to good agreement with the densities of OH, O and H measured in radio-frequency driven plasma sources, operated in several different geometries, at atmospheric pressure as described in detail elsewhere [98, 99, 101]. In this use case, the chemical reduction and subsequent analysis are carried out in two steps:

- Simulations using the full reaction set are carried out using the QGM in conjunction with the chemical reduction method described in [59].

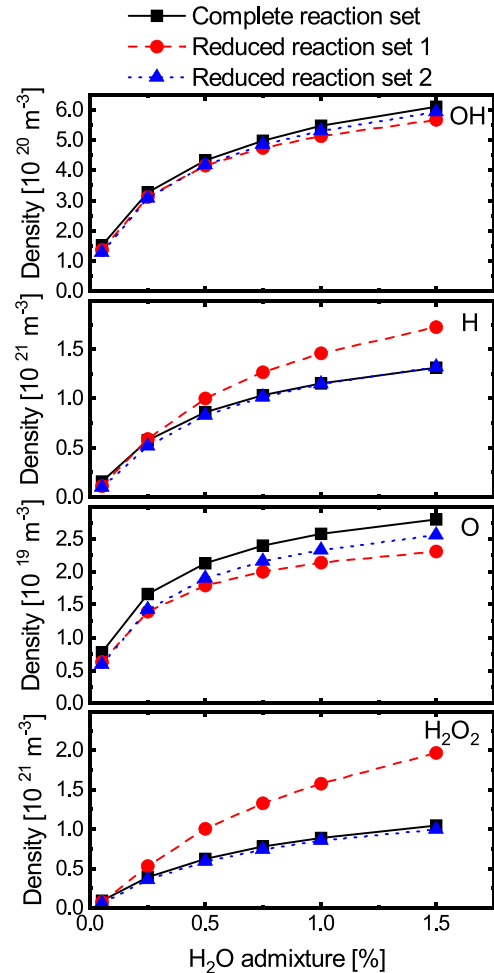
Table 4. Summary of the three reaction sets used in this section, and the model outputs that should remain fixed when comparing the original and RRSs.

	Complete reaction set	RRS 1	RRS 2
Fixed quantities	N.A.	$T_e, n_e, n_O, n_H, n_{OH}$	$T_e, n_e, n_O, n_H, n_{OH}, n_{HO_2}, n_{H_2O_2}$
No. species	46	18	18
No. reactions	577	90	93

- Simulations using the RRSs are carried out using GlobalKin.

Reduction of the complete reaction set is carried out for conditions equivalent to those used in figure 7 of [98], where OH densities are measured and simulated as a function of distance along the channel of the plasma source, in the direction of the gas flow. Briefly, the plasma jet used in that work employs a plane-parallel electrode configuration with an electrode separation of 1 mm and electrode areas of (11 × 30) mm. Simulations are carried out using a power-per-unit volume of 18 W cm⁻³. The gas mixture consisted of He at atmospheric pressure with a water vapor fraction of 0.54% ppm. In [98], pathway analysis demonstrated that the production and consumption processes of OH vary as a function of distance along the gas flow. In order to account for this in the chemical reduction, both the species ranking and the evaluation of the reduced sets with regard to the error induced by removing one species was carried out taking one point in the steady-state regime and one in the regime close to the gas inflow. It should be noted that QGM solves in the time-domain in contrast to the quasi one-dimensional plug flow simulations in GlobalKin; however, this should have limited bearing on the reduction. The criteria used in the reduction consist of a number of simulation outputs that should remain unchanged, in this case to within 10%, before and after reduction. Here, two reductions were carried out. The criteria used for each reduction, as well as the number of species and reactions in the complete and RRSs are summarised in table 4.

After completing the reduction process, GlobalKin simulations are carried out, as described in reference [98], with the complete reaction set and each RRS for a variety of different H₂O admixtures. For these simulations, the power deposition and plasma dimensions are slightly different to those used in the reduction process. These modified conditions correspond to the those for which OH densities are measured at a fixed location within the plasma jet as a function of H₂O admixture, as presented in figure 9 of reference [98]. The densities of several important plasma-produced reactive species in the mixture, OH, H, O and H₂O₂, predicted by each reaction set are shown in figure 12, which shows that the densities of OH, H and O are well reproduced by both RRSs for H₂O admixtures of close to 0.5%. This is expected since the reduction of the complete reaction set is carried out for a gas mixture of ≈0.5% and the densities of OH, H and O are all constrained in the reduction process. For OH and O, the agreement between the complete reaction set and both the reduced sets remains good for all admixtures considered. However, the H densities predicted by the RRS 1 begin to diverge from the complete reaction set for higher H₂O admixtures. In the case of H₂O₂,

**Figure 12.** Densities of OH, H, O, H₂O₂ at a distance of 2 cm from the start of the plasma channel, as a function of H₂O admixture for the complete reaction set and both RRSs. Power per unit volume = 14 W cm⁻³.

good agreement is also obtained between the complete reaction set both RRSs for H₂O admixtures of close to 0.5%, despite the fact that it is not specifically constrained by the reduction process for RRS 1. However, as for H, the H₂O₂ density predicted by RRS 1 diverges from that predicted by the complete reaction set at higher H₂O admixtures.

Based on these results, it is clear that the reduction procedure succeeds in generating RRSs that preserve the densities of the constrained species close to the conditions under which the reduction is carried out and that this reduction transfers well between different global models. RRS 2 also allows for a successful prediction of the densities of all species considered over a wider range of admixtures. However, while RRS 1 allows for the OH and O densities to be reproduced over a

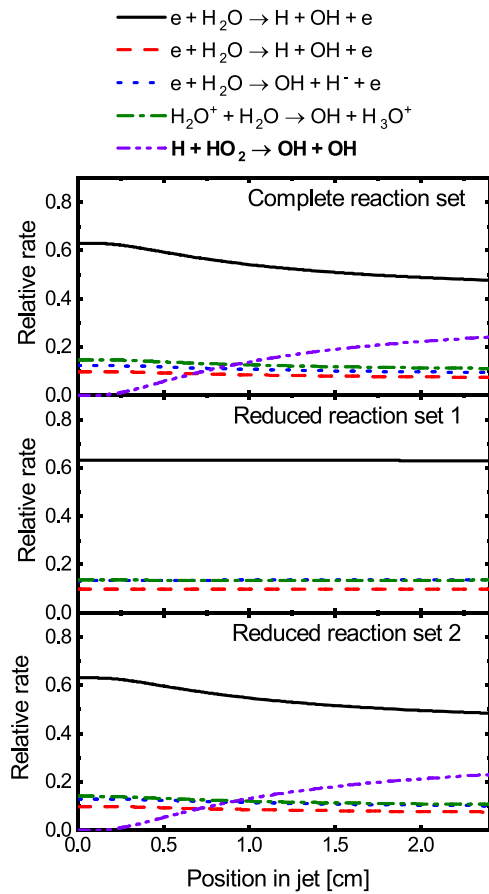


Figure 13. Relative rates of the major production processes of OH as a function of distance from the start of the plasma channel for the complete reaction set and both RRSs. H₂O admixture = 0.5%, power per unit volume = 14 W cm⁻³. The reaction highlighted in bold denotes a process that is present in the complete reaction set and RRS 2, but not RRS 1.

wider range, the densities of H and H₂O₂ diverge from the correct solution at higher admixtures.

To obtain greater insight into the origin of these results, the production and consumption pathways of OH are presented in figures 13 and 14. In figure 13, it is observed that RRS 2 reproduces the production pathways of OH found in the complete reaction set almost exactly. For the RRS 1, differences are found when compared to the complete reaction set. Most importantly, reduction 1 leads to the removal of HO₂ from the reaction mechanism, which in turn removes the reaction:



Since this reaction plays an increasingly important role in OH formation with increasing distance from the start of the plasma channel, the overall production pathway for OH is changed significantly in comparison to the complete reaction set, even though its density is still preserved.

From the perspective of OH consumption, shown in figure 14, similar observations can be made. In this case, the RRS 2 also reproduces the consumption pathways of OH found in the complete reaction set almost exactly. However, the absence of HO₂ from the RRS 1 leads to the omission of

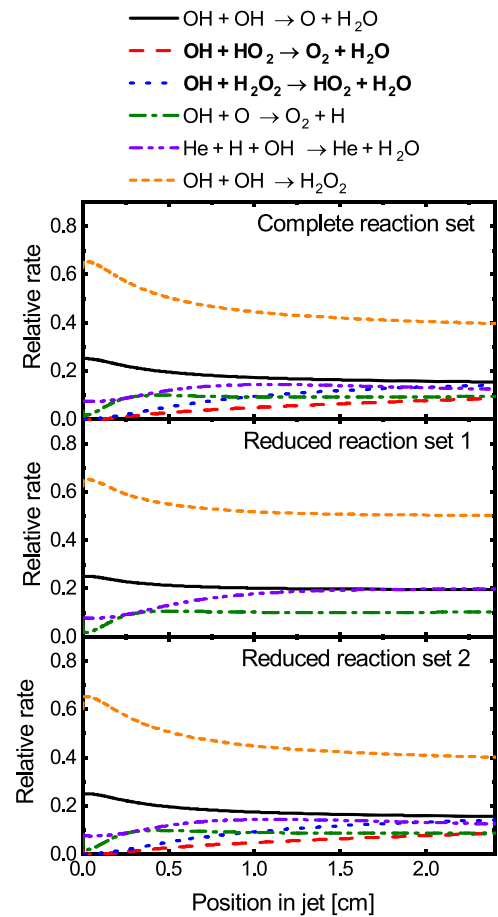
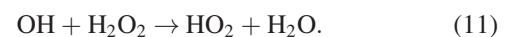
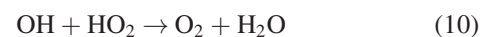


Figure 14. Relative rates of the major consumption processes of OH as a function of distance from the start of the plasma channel for the complete reaction set and both RRSs. H₂O admixture = 0.5%, power per unit volume = 14 W cm⁻³. The reactions highlighted in bold denote processes that are present in the complete reaction set and RRS 2, but not RRS 1.

two important OH consumption processes:



As for the production, the omission of these processes modifies the overall consumption dynamic of OH.

From analysis of the production and consumption pathways it can be observed that it is possible to reproduce the densities of OH very accurately using a reaction set that is fundamentally incomplete (RRS 1). In this case, this is made possible due to the similar contributions of HO₂ to the production and consumption processes of OH, such that when HO₂ is neglected in the reaction set the net effect on the OH density is negligible, under these specific conditions. In general, this underlines the complex nature of model reduction and the importance of comparing formation pathways of important species before and after chemical reduction, in addition to species densities.

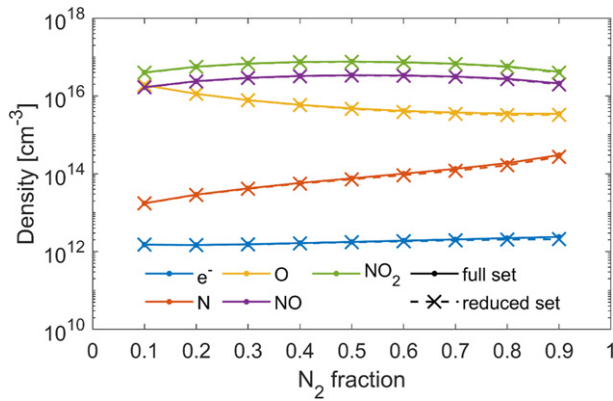


Figure 15. Comparison of the full and reduced chemistry sets for different N_2 fractions in the feed gas, as calculated with ZDPlasKin.

4.4. Vibrationally-resolved air chemistry and chemistry reduction

A new chemistry added to the database describes nitrogen/oxygen mixtures [102–104]. This set contains 82 different species and 4663 reactions. The species include also 24 and 15 vibrational levels of N_2 and O_2 , respectively. The vibrational interactions account for 88% of all the reactions. It should be noted that the temperature-dependent rate coefficients of these reactions are not given standard Arrhenius form. These reactions are not included in QDB for the time being but will be added once QDB support for other formats for temperature-dependent rate coefficients is implemented. This chemistry set was used in combination with the zero-dimensional plasma kinetics solver (ZDPlasKin) 0D plasma kinetics solver, which yielded good agreement with experiments for a wide range of conditions and at various feed gas ratios [102–104]. In this example case, we show how one might take a chemistry from the QDB for their own modeling purposes, by means of an initial exploratory study of a different plasma system. The gas phase of a DC driven micro-plasma over water [105] is modeled using the same ZDPlasKin modeling platform. In addition, we show the potential of the chemistry reduction, which will be incorporated into the QDB in the future. The full chemistry and the ZDPlasKin model are briefly described.

4.4.1. Brief summary of the chemistry set. The chemistry set was compiled from various sources. The neutral–neutral and ion–neutral collisions are generally described by rate coefficient expression taken from literature, as described in detail before [102]. The electron impact collisions are described by cross sections mainly taken from the LXCat database [2]. Specifically, the electron impact vibrational (de-)excitation cross sections were taken from the Phys4Entry database instead [7]. Furthermore, the N_2 – N_2 , O_2 – O_2 and N_2 – O_2 vibrational–vibrational relaxations and N_2 – N_2 , O_2 – O_2 , N_2 – O_2 and O_2 – N_2 vibrational–translational (VT) relaxations by Adamovich [106] are included in the chemistry, as well as the VT relaxations of N_2 – N and O_2 – O by Esposito [107, 108] and the VT relaxation of N_2 – O after Guerra and Gordiets [87, 109–114].

4.4.2. ZDPlasKin model setup and comparison against QGM. ZDPlasKin is a FORTRAN 90 based modeling platform to describe non-thermal plasma with complex chemistry [115]. Typically, users write their own master code which incorporates most of the physics. This gives relative freedom to describe a specific plasma system. The master code interacts with the ZDPlasKin module which handles solving the differential equations as well as the coupling with BOLSIG+, the incorporated numerical solver of the Boltzmann equation for the electrons [116]. The DC driven micro-plasma [105] is chosen to be modeled as a simple control volume with perfect mixing in which all species reside only for a short time. The continuity equation then becomes

$$\frac{dn_i}{dt} = \left(\frac{\delta n_i}{\delta t} \right)_{\text{vol}} + \frac{1}{\tau_{\text{res}}} n_{i,0} - \frac{1}{\tau_{\text{res}}} \frac{P}{P_0} n_i, \quad (12)$$

where P and P_0 are the current and initial pressures, respectively. This equation corresponds to volumetric reactions and flow terms of the QGM equation (A.1). However, here we directly set the residence time and the pressure recovery time scale is set equal to this residence time. In addition, unlike in the QGM, this equation is also solved for the electron density and the electron impact rate coefficients are evaluated directly from the EEDF calculated by the coupled Boltzmann solver BOLSIG+. ZDPlasKin does not have an explicit equation to calculate the electron energy (density), instead, the electron energy is the mean electron energy evaluated from the EEDF. To calculate the EEDF from the Boltzmann equation, a (reduced) electric field is required, calculated with [117]

$$\frac{E}{N} = \frac{1}{N} \sqrt{\frac{P/V}{e\mu_e n_e}}, \quad (13)$$

where $\frac{E}{N}$ is the reduced electric field, N is the gas density and $\frac{P}{V}$ is the plasma power density. The electron mobility, μ_e , is calculated from the (previous) EEDF. This equation assumes that all the plasma power goes into Joule heating of the electrons, and this power principally corresponds to the first term in equation (A.28). ZDPlasKin can also self-consistently calculate the gas temperature, however a fixed gas temperature of 1231 K was chosen based on the experimental setup described. A constant plasma power density of 6276 W cm^{-3} is used. This corresponds to the experimental plasma, operated at low current. An estimated residence time of 1 ms was chosen based on the small plasma volume [105]. The model is solved until steady state is reached.

4.4.3. Results and discussion. The calculations were performed for gas mixtures ranging from 10/90 to 90/10% N_2/O_2 . The reduction was done based on a selected condition (10/90% N_2/O_2) and with a focus on N and O atoms and NO and NO_2 molecules as the species of interest. The removal of a species from the chemistry was only allowed to change the density of the species of interest by 1%. 38 species could be removed, most of which were ions and electronically excited states. Vibrational levels above the 19th and 5th level of nitrogen and oxygen could also be removed, respectively. This led to the

removal of 2571 reactions, 2313 of which involved vibrational levels. Hence, compared to the full set, which consists of 82 different species and 4663 reactions, the reduced set only contains 44 different species and 2350 reactions. In other words, the number of reactions was reduced by 55%. This reduction was found to translate well to the other feed gas ratios. Less restrictive reductions, for example allowing up to 10% change, did not translate equally well to the other feed gas ratios. The resulting electron, N, O, NO and NO₂ densities calculated with the full and reduced chemistry are plotted in figure 15. The reduced chemistry gives significantly improved calculation times (30%–40% faster).

5. Conclusions and future developments

This is the second formal release of the QDB which has seen a significant increase in both the data and functionality provided since the original release in 2017 [10]. It is our intention to continue to expand both features and, in particular, we would welcome any contribution of appropriate data from scientists interested in distributing their results via QDB. We are also exploring the use of machine learning to fill in gaps in knowledge of reactions. However, as the use cases aim to demonstrate, the reactions sets in QDB already provide the necessary data for modeling a range of different plasmas.

This study also illustrates the usefulness of reducing the size of chemistries. In the future we plan to integrate the ranking-based iterative reduction method of Hanicinec *et al* [59] for automatic selection of relevant species in the chemistry generator as a desktop application of QDB. Our tests above suggest that this reduction works well. Similarly we are aiming for the complete integration of the Boltzmann-solver and QGM. At present the treatment of surface processes remains rather rudimentary and we hope to integrate a site-based surface model with QGM global model, including allowing for self-consistent calculation of surface coefficients used in the plasma model. A further extension of this approach would be the automatic calibration of surface coefficients and unknown rate coefficients to match experimental data.

One new direction we are currently exploring is the role of radiative processes in plasmas. In low pressure plasmas radiative decay of excited states can lead to significant changes in the state populations. We are currently constructing a new lifetime database (LiDa) which will provide information on both lifetimes and radiative decay pathways. For molecules these data are being assembled from the very extensive spectroscopic data for hot molecules provided by the ExoMol database [22].

Acknowledgments

We thank Uwe Czarnetzki, Daniel B Brown, Maria Tudorovskaya, Bridgette Cooper, Peter J Bruggeman, Bastiaan J Braams, Matthew J Goeckner, Alok Ranjan, Geoff Hassall, Khaled Hassouni, E Krishnakumar, Mark J Kushner, Annarita Laricchiuta, Yi-Kang Pu, Julian Schulze,

Jung-Sik Yoon, Mi-Young Song, and Nigel Mason, for their contributions to and helpful discussions during this project. Partial funding was received from the UK STFC under Grants ST/M007774 and ST/K004069. Martin Hanicinec would like to thank EPSRC for a CASE studentship under Grant EP/N509577/1. The work of Klaus Bartschat, Kathryn Hamilton, and Oleg Zatsarinny was supported by the United States National Science Foundation under Grants PHY-1803844, OAC-1834740, PHY-2110023, and the XSEDE allocation PHY-090031. The work of Luís L Alves was partially funded by the Portuguese FCT—Fundação para a Ciência e a Tecnologia, under projects UIDB/50010/2020 and UIDP/50010/2020.

Data availability statement

The reactions and species data discussed in this article are available via the QDB database which can be accessed at <http://quantemoldb.com>.

Appendix A. Quantemol global model

This section explicitly describes the equations being solved for in the QGM. For clarity, Table A1 summarises all the symbols and quantities used in this section.

Particle density balance equation:

The time derivative of all heavy species densities is expressed as a sum of contributions from volumetric processes, flow sources and sinks and surface (diffusion) processes:

$$\frac{dn_i}{dt} = \left(\frac{\delta n_i}{\delta t}\right)_{\text{vol}} + \left(\frac{\delta n_i}{\delta t}\right)_{\text{flow}} + \left(\frac{\delta n_i}{\delta t}\right)_{\text{diff}}. \quad (\text{A.1})$$

The contribution of volumetric reactions is

$$\left(\frac{\delta n_i}{\delta t}\right)_{\text{vol}} = \sum_j (a_{ij}^{\text{R}} - a_{ij}^{\text{L}}) k_j \prod_l n_{lj}^{\text{L}} = \sum_j (a_{ij}^{\text{R}} - a_{ij}^{\text{L}}) R_j, \quad (\text{A.2})$$

where n_{lj}^{L} is the density of l th species on the left-hand side of reaction j . The reaction rate coefficient k_j takes form of the modified Arrhenius equation

$$k_j = A_j \left(\frac{T_g}{300 \text{ K}}\right)^{n_j} \exp\left(-\frac{E_{a,j}}{T_g}\right) \quad (\text{A.3})$$

for heavy species reactions j (reactions where all the reactants are heavy species) and

$$k_j = A_j \left(\frac{T_e}{1 \text{ eV}}\right)^{n_j} \exp\left(-\frac{E_{a,j}}{T_e}\right) \quad (\text{A.4})$$

for electron processes j (reactions where at least one reactant is an electron). The Arrhenius parameters A_j , n_j and $E_{a,j}$ (or $E_{a,j}$) describe the collisional kinetics of the model.

The contribution of flow to the time evolution of heavy species densities will consist of inflow and outflow terms as well as a term regulating the pressure.

Table A1. Summary of symbols used for the documentation of the global model presented.

Symbol	Unit	Description
i, k		Index, running over species in a kinetic scheme
i_0, i_+, i_-		Indices i running over neutral, positive and negative species respectively
j		Index, running over reactions in a kinetic scheme
N_S		Number of species in a kinetic scheme
n_i	m^{-3}	Number density of the i th species in a kinetic scheme
n_e	m^{-3}	Electron number density
ϱ_e	$eV m^{-3}$	Electron energy density
P	W	Absorbed power
p_0	Pa	Desired pressure
p	Pa	Instantaneous pressure
Q_i	sccm	Feed flow for i th species in a kinetic scheme
R_p, Z_p	m	Plasma dimensions: radius and length
V	m^3	Plasma volume
T_g	K	Neutral temperature
T_i	K	Positive ion temperature
T_e	eV	Electron temperature
k_j	$m^{-3+3m} s^{-1}$	Reaction rate coefficient of the j th reaction of an order m in a kinetic scheme
R_j	$m^{-3} s^{-1}$	Reaction rate of the j th reaction in a kinetic scheme
$M_{cp,j}$	kg	Mass of the collision partner in j th electron reaction
M_i	kg	Mass of the i th species
m_e	kg	Electron mass
q_i	e	Charge of the i th species
e	C	Electron charge
σ_i^{LJ}	m	σ parameter of the Lennard-Jones potential for i th species
$\Delta E_{e,j}^{inel}$	eV	Electron energy loss due to an inelastic collision j
a_{ij}^L		Stoichiometric coefficient of i th distinct species on left-hand side in j th reaction
a_{ij}^R		Stoichiometric coefficient of i th distinct species on right-hand side in j th reaction
a_{ij}		Net stoichiometric coefficient of i th distinct species in j th reaction
A_j	$m^{-3+3m} s^{-1}$	Arrhenius parameter—pre-exponential factor
n_j		Arrhenius parameter—exponent
$E_{a,j}$	eV	Arrhenius parameter—activation energy
$E_{a,j}$	K	Arrhenius parameter—activation energy
k_B	J K ⁻¹	Boltzmann constant
s_i		Sticking coefficient—probability of i th species sticking to a plasma boundary ($s_i \in [0, 1]$)
r_{ik}		Return coefficient—number of i th species returned for each <i>one</i> of <i>stuckk</i> th species ($r_{ik} \in \mathbf{R}_0^+$)
D_i	$m^2 s^{-1}$	Diffusion coefficient of i th species
D_a	$m^2 s^{-1}$	Ambipolar diffusion coefficient
Λ	m	Characteristic diffusion length
λ_i	m	Mean free path of i th species
\bar{v}_i	$m s^{-1}$	Mean speed of i th species
σ_{ik}^m	m^2	Momentum transfer cross section for i th species scattering on k th species
V_s	V	Mean sheath voltage
n_{min}	m^{-3}	Minimal allowed particle density
$\varrho_{e,min}$	$eV m^{-3}$	Minimal allowed electron energy density

$$\left(\frac{\delta n_i}{\delta t}\right)_{flow} = \left(\frac{\delta n_i}{\delta t}\right)_{flow}^{in} + \left(\frac{\delta n_i}{\delta t}\right)_{flow}^{out} + \left(\frac{\delta n_i}{\delta t}\right)_{flow}^{reg}. \quad (A.5)$$

The inflow is expressed as

$$\left(\frac{\delta n_i}{\delta t}\right)_{flow}^{in} = \frac{Q'_i}{V}, \quad (A.6)$$

where

$$Q'_i = \frac{N_A}{V_m \cdot 60} Q_i = 4.478 \times 10^{17} \cdot Q_i \quad (A.7)$$

is the inflow expressed in (particles s^{-1}) rather than in (sccm). $N_A = 6.022 \times 10^{23} \text{ mol}^{-1}$ is Avogadro constant and $V_m =$

$2.241 \times 10^4 \text{ cm}^3 \text{ mol}^{-1}$ is the molar volume for ideal gas at standard temperature and pressure. The outflow term is set in such a way that only neutrals are leaving the plasma region due to the flow, the neutral species flow rate is proportional to the species density and the total flow rate out of the plasma region is the same as total inflow rate:

$$\left(\frac{\delta n_i}{\delta t}\right)_{flow}^{out} = \begin{cases} -\frac{\sum Q'_i}{\sum n_{i_0}} \cdot \frac{n_i}{V} & \text{neutrals,} \\ 0 & \text{ions,} \end{cases} \quad (A.8)$$

where the index i_0 runs only over neutral species. And the term regulating the plasma pressure is added to the particle

balance equation, accounting for changes in p due to dissociation/association processes and to diffusion losses and surface sources. This term, similarly to the outflow term, only acts upon the neutral species and can be viewed as an addition to the outflow term, or physically as adjusting a pressure-regulation valve between a plasma chamber and a pump, based on the instantaneous pressure.

$$\left(\frac{\delta n_i}{\delta t}\right)_{\text{flow}}^{\text{reg}} = \begin{cases} -\frac{p-p_0}{p_0} \frac{n_i}{\tau_p} & \text{neutrals,} \\ 0 & \text{ions.} \end{cases} \quad (\text{A.9})$$

Here, p is the instantaneous pressure from the state equation for an ideal gas

$$p = k_B T_g \cdot \sum_i n_i, \quad (\text{A.10})$$

and τ_p is a pressure recovery time scale. A value of $\tau_p = 10^{-3}$ s was found to yield satisfactory results for a wide range of process parameters.

The diffusion contribution toward the particle balance equation is ultimately controlled by the vector of sticking coefficients s_i and matrix of return coefficients r_{ik} and the diffusion model:

$$\left(\frac{\delta n_i}{\delta t}\right)_{\text{diff}} = \left(\frac{\delta n_i}{\delta t}\right)_{\text{diff}}^{\text{out}} + \left(\frac{\delta n_i}{\delta t}\right)_{\text{diff}}^{\text{in}}. \quad (\text{A.11})$$

The rate of species loss to the plasma boundaries due to diffusion is expressed as

$$\left(\frac{\delta n_i}{\delta t}\right)_{\text{diff}}^{\text{out}} = \frac{A}{V} \Gamma_{\text{wall},i}, \quad (\text{A.12})$$

where V and A are plasma volume and plasma boundaries area respectively, while the wall fluxes $\Gamma_{\text{wall},i}$, as used (among others) by Kushner in GlobalKin [118], is expressed as

$$\Gamma_{\text{wall},i} = -\frac{D_i n_i s_i}{s_i \Lambda + \frac{4D_i}{\bar{v}_i}} \quad (\text{A.13})$$

where

$$\Lambda = \left[\left(\frac{\pi}{Z_p}\right)^2 + \left(\frac{2.405}{R_p}\right)^2 \right]^{-1/2}. \quad (\text{A.14})$$

The diffusion coefficient is calculated separately for neutrals and ions. For positive and negative ions, the diffusion coefficient is the coefficient of ambipolar diffusion in electronegative plasma, as proposed by Stoeffels *et al* in [91].

$$D_i = \begin{cases} D_i^{\text{free}} & \text{neutrals,} \\ D_+^{\text{free}} \frac{1 + \gamma(1 + 2\alpha)}{1 + \alpha\gamma} & \text{+ions,} \\ 0 & \text{-ions.} \end{cases} \quad (\text{A.15})$$

Here, $\gamma = T_e/T_i$ and $\alpha = \sum n_{i^-}/n_e$. $D_i = 0$ for negative ions implies that no negative ions are reaching the plasma boundaries and therefore there are no negative ion diffusion losses. This approximation is justified by the positive plasma potential trapping the negative ions in the plasma bulk. It should be noted that the stated ambipolar diffusion coefficients are only

valid for the case of $\alpha \ll \mu_e/\mu_i$, where μ are mobilities of electrons and ions respectively. The free diffusion coefficient for heavy species is calculated as

$$D_i^{\text{free}} = \frac{\pi}{8} \lambda_i \bar{v}_i. \quad (\text{A.16})$$

The mean free path λ_i for all heavy species is

$$\frac{1}{\lambda_i} = \sum_k n_k \sigma_{ik}^m (1 - \delta_{ik}), \quad (\text{A.17})$$

where σ_{ik}^m is the momentum transfer cross section, and the mean speed \bar{v}_i is the mean thermal speed

$$\bar{v}_i = \begin{cases} \left(\frac{8k_B T_g}{\pi M_i}\right)^{1/2} & \text{neutrals,} \\ \left(\frac{8k_B T_i}{\pi M_i}\right)^{1/2} & \text{ions,} \end{cases} \quad (\text{A.18})$$

where the ion temperature is approximated, as proposed by Lee and Lieberman in [119], by

$$T_i = \begin{cases} (5800 - T_g) \frac{0.133}{p} + T_g & p > 0.133 \text{ Pa,} \\ 5800 & p \leq 0.133 \text{ Pa.} \end{cases} \quad (\text{A.19})$$

The momentum transfer cross section σ_{ik}^m is for the purpose of this model crudely approximated with hard sphere model for neutral–neutral and ion–neutral collisions, and with momentum transfer for Rutherford scattering (as proposed by Lieberman and Lichtenberg in [120]) for the case of ion–ion collisions:

$$\sigma_{ik}^m = \begin{cases} (\sigma_i^{\text{LJ}} + \sigma_k^{\text{LJ}})^2 & i = i_+, i_-, i_0, \text{ and } k = k_0, \\ & i = i_0, \text{ and } k = k_+, k_-, \\ \pi b_0^2 \ln\left(\frac{2\lambda_{\text{De}}}{b_0}\right) & i = i_+, i_-, \text{ and } k = k_+, k_-, \end{cases} \quad (\text{A.20})$$

with Debye length

$$\lambda_{\text{De}} = \left(\frac{\epsilon_0 T_e}{en_e}\right)^{1/2}, \quad (\text{A.21})$$

classical distance of closest approach

$$b_0 = \frac{q_i q_k e^2}{2\pi \epsilon_0 m_R v_R^2}, \quad (\text{A.22})$$

reduced mass

$$m_R = \frac{m_i m_k}{m_i + m_k}, \quad (\text{A.23})$$

and the relative speed being approximated by the mean thermal speed

$$v_R = \bar{v}_i. \quad (\text{A.24})$$

The δ_{ik} term filters out self-collisions, as collisions between the same species do not affect the species collective behavior

$$\delta_{ik} = \begin{cases} 1 & \text{for } i = k, \\ 0 & \text{for } i \neq k. \end{cases} \quad (\text{A.25})$$

Table B1. Summary of neutral, unstateful species currently contained in QDB. Also given is the availability of electron collision data (column A) and heavy particle reaction rates (column B).

	A	B		A	B		A	B		A	B		A	B		A	B
Al	✓	✓	C ₃ F ₅	✓	✓	C ₅ H ₉	×	×	CF ₄	×	×	F ₂ O	✓	×	NP	×	✓
AlO	×	×	C ₃ F ₆	✓	✓	C ₅ HN	×	✓	CF ₄	✓	✓	F ₃	×	×	NS	×	✓
Ar	✓	✓	C ₃ F ₇	✓	✓	C ₅ N	×	✓	CH	✓	✓	F ₄	×	×	NSi	×	✓
B	✓	✓	C ₃ F ₈	✓	×	C ₅ O	×	✓	CH ₂	✓	✓	FNO	×	✓	Na	×	✓
BCl	✓	✓	C ₃ H	✓	✓	C ₅ S	×	×	CH ₂ F	×	✓	FO	×	✓	Ne	✓	×
BCl ₂	✓	✓	C ₃ H ₂	✓	✓	C ₆	✓	✓	CH ₂ F ₂	✓	✓	FO ₂	×	✓	O	✓	✓
BCl ₃	✓	✓	C ₃ H ₂ N	×	✓	C ₆ H	✓	✓	CH ₂ N ₂	×	✓	Fe	×	✓	O ₂	×	×
BF	✓	×	C ₃ H ₂ O	×	✓	C ₆ H ₁₀	×	×	CH ₂ NS	×	×	FeH	×	×	O ₂	✓	✓
BF ₂	✓	×	C ₃ H ₂ S	×	✓	C ₆ H ₁₂	×	×	CH ₂ O ₂	×	✓	H	✓	✓	O ₃	✓	✓
BF ₃	✓	×	C ₃ H ₃	✓	✓	C ₆ H ₁₃	×	×	CH ₂ S	×	✓	H ₂	✓	✓	O ₃ S	×	×
BeH	×	×	C ₃ H ₃ N	×	✓	C ₆ H ₁₄	×	×	CH ₂ Si	×	✓	H ₂	×	×	OH	✓	✓
BeH ₂	✓	×	C ₃ H ₃ Si	×	×	C ₆ H ₂	×	✓	CH ₃	✓	✓	H ₂ CN	×	✓	OP	×	✓
Br	✓	✓	C ₃ H ₄	✓	✓	C ₆ H ₃	×	✓	CH ₃ F	✓	✓	H ₂ Mg	×	×	OS	×	✓
Br ₂	✓	✓	C ₃ H ₄ O	×	×	C ₆ H ₃ N	×	✓	CH ₃ N	×	✓	H ₂ O	×	×	P	×	✓
BrCl	×	✓	C ₃ H ₅	✓	✓	C ₆ H ₄	×	×	CH ₃ NS	×	✓	H ₂ O	✓	✓	PH ₃	✓	×
C	✓	✓	C ₃ H ₅ N	×	✓	C ₆ H ₅	×	✓	CH ₃ O	×	✓	H ₂ O ₂	×	✓	S	✓	✓
C ₁₀	✓	✓	C ₃ H ₅ Si	×	×	C ₆ H ₆	×	✓	CH ₃ P	×	✓	H ₂ OS	×	×	S ₂	×	✓
C ₁₀ H	✓	✓	C ₃ H ₆	✓	✓	C ₆ H ₇	×	×	CH ₃ S	×	✓	H ₂ P	×	✓	SF	✓	✓
C ₁₀ H ₂	×	✓	C ₃ H ₆ O	×	✓	C ₆ H ₈	×	×	CH ₃ Si	×	✓	H ₂ S	✓	✓	SF ₂	✓	✓
C ₁₀ N	×	✓	C ₃ H ₇	✓	✓	C ₆ H ₉	×	×	CH ₄	×	×	H ₂ S ₂	×	✓	SF ₃	✓	✓
C ₁₁	×	✓	C ₃ H ₈	✓	✓	C ₆ HN	×	✓	CH ₄	✓	✓	H ₃	×	×	SF ₄	✓	✓
C ₁₂	×	×	C ₃ HN	✓	✓	C ₆ HSi	×	×	CH ₄ N	×	✓	H ₄	×	×	SF ₅	✓	✓
C ₁₂ H	×	✓	C ₃ HO	×	✓	C ₆ N	×	✓	CH ₄ NS	×	×	HBr	✓	✓	SF ₆	×	×
C ₁₂ H ₂	×	×	C ₃ HS	×	✓	C ₆ N ₂	×	✓	CH ₄ O	×	✓	HCHO	✓	✓	SF ₆	✓	✓
C ₁₄ H ₁₀	×	✓	C ₃ HSi	×	✓	C ₇	✓	✓	CH ₄ S	×	✓	HCN	✓	✓	SO ₂	✓	✓
C ₂	✓	✓	C ₃ N	✓	✓	C ₇ H	✓	✓	CH ₅ N	×	✓	HCP	✓	✓	SO ₂ F ₂	×	✓
C ₂ F ₂	×	×	C ₃ O	×	✓	C ₇ H ₁₀	×	×	CH ₅ NS	×	✓	HCl	✓	✓	SOF	×	✓
C ₂ F ₃	✓	✓	C ₃ P	×	✓	C ₇ H ₂	×	✓	CHF	✓	✓	HF	✓	✓	SOF ₂	×	✓
C ₂ F ₄	✓	✓	C ₃ S	×	✓	C ₇ H ₃	×	×	CHF ₂	✓	✓	HMg	×	✓	SOF ₃	×	✓
C ₂ F ₅	✓	✓	C ₃ Si	×	✓	C ₇ H ₄	×	✓	CHF ₃	✓	✓	HNO	×	✓	SOF ₄	×	✓
C ₂ F ₆	✓	✓	C ₄	✓	✓	C ₇ H ₅	×	×	CHF ₃	×	×	HNSi	×	✓	SSi	×	✓
C ₂ H	✓	✓	C ₄ F ₆	✓	×	C ₇ H ₆	×	×	CHNO	×	✓	HNa	×	✓	Si	✓	✓
C ₂ H ₂	✓	✓	C ₄ F ₇	✓	✓	C ₇ H ₇	×	×	CHNS	×	✓	HNaO	×	×	Si ₂ H ₄	×	×
C ₂ H ₂ N	×	✓	C ₄ F ₈	✓	✓	C ₇ H ₈	×	×	CHO	×	✓	HO ₂	×	✓	Si ₂ H ₅	×	✓
C ₂ H ₂ O	×	✓	C ₄ H	✓	✓	C ₇ H ₉	×	×	CHO ₂	×	×	HO ₂ NO ₂	×	✓	Si ₂ H ₆	✓	✓
C ₂ H ₂ O ₂	×	×	C ₄ H ₁₀	×	✓	C ₇ HN	×	✓	CHS	×	✓	HONO	×	✓	Si ₃ H ₇	×	×
C ₂ H ₂ S	×	✓	C ₄ H ₂	×	✓	C ₇ N	×	✓	CHSi	×	✓	HONO ₂	×	✓	Si ₃ H ₈	×	✓
C ₂ H ₂ Si	×	✓	C ₄ H ₂ N	×	×	C ₇ O	×	✓	CN	×	✓	HOP	×	✓	Si ₄ H ₁₀	×	✓
C ₂ H ₃	✓	✓	C ₄ H ₃	×	✓	C ₈	✓	✓	CN ₂	×	×	HOS	×	×	Si ₄ H ₉	×	×
C ₂ H ₃ N	×	✓	C ₄ H ₃ N	×	✓	C ₈ H	✓	✓	CNO	×	✓	HP	×	✓	Si ₅ H ₁₁	×	×
C ₂ H ₃ NO	×	✓	C ₄ H ₄	×	✓	C ₈ H ₂	×	✓	CNSi	×	✓	HS	×	✓	Si ₅ H ₁₂	×	✓
C ₂ H ₃ O	×	✓	C ₄ H ₅	×	✓	C ₈ H ₃	×	×	CO	✓	✓	HS ₂	×	✓	Si ₆ H ₁₃	×	×
C ₂ H ₃ Si	×	×	C ₄ H ₅ N	×	×	C ₈ H ₃ N	×	✓	CO ₂	✓	✓	He	✓	✓	Si ₆ H ₁₄	×	✓
C ₂ H ₄	✓	✓	C ₄ H ₆	×	✓	C ₈ H ₄	×	×	CO ₂	×	×	Hg	✓	×	Si ₇ H ₁₅	×	×
C ₂ H ₄ O	×	✓	C ₄ H ₇	×	×	C ₈ H ₆	×	×	COF	✓	✓	I	×	×	Si ₇ H ₁₆	×	✓
C ₂ H ₄ O ₂	×	✓	C ₄ H ₈	×	✓	C ₈ HN	×	✓	COF ₂	✓	✓	Kr	✓	×	Si ₈ H ₁₇	×	×
C ₂ H ₄ S	×	✓	C ₄ H ₉	×	×	C ₈ HSi	×	×	CONH ₃	✓	✓	M	✓	✓	Si ₈ H ₁₈	×	✓
C ₂ H ₅	✓	✓	C ₄ HN	×	✓	C ₈ N	×	✓	COS	✓	✓	Mg	×	✓	Si ₉ H ₂₀	×	×
C ₂ H ₅ N	×	×	C ₄ HSi	×	×	C ₈ N ₂	×	✓	CP	×	✓	N	×	✓	SiCl	×	×
C ₂ H ₅ O	×	✓	C ₄ N	×	✓	C ₉	✓	✓	CS	✓	✓	N ₂	✓	✓	SiCl ₂	✓	×
C ₂ H ₆	✓	✓	C ₄ N ₂	×	✓	C ₉ H	✓	✓	CSi	×	✓	N ₂	×	×	SiCl ₃	×	×
C ₂ HN	×	✓	C ₄ P	×	✓	C ₉ H ₂	×	✓	CaF	✓	×	N ₂ H	×	✓	SiCl ₄	×	×
C ₂ HN ₂	×	✓	C ₄ S	×	✓	C ₉ H ₃	×	×	Cl	✓	✓	N ₂ H ₂	×	✓	SiF	×	×
C ₂ HO	×	✓	C ₄ Si	×	✓	C ₉ H ₄	×	×	Cl ₂	✓	✓	N ₂ H ₃	×	✓	SiF ₂	✓	×
C ₂ HO ₂	×	×	C ₅	✓	✓	C ₉ HN	×	✓	ClHO	×	✓	N ₂ H ₄	×	✓	SiF ₃	✓	×
C ₂ HP	×	✓	C ₅ H	✓	✓	C ₉ N	×	✓	ClO	✓	✓	N ₂ O	✓	✓	SiF ₄	✓	×
C ₂ HS	×	✓	C ₅ H ₁₀	×	×	C ₉ O	×	✓	ClO ₂	×	✓	N ₂ O ₃	×	✓	SiH	✓	✓
C ₂ HSi	×	✓	C ₅ H ₁₂	×	×	CCl	×	✓	ClS	×	×	N ₂ O ₄	×	✓	SiH ₂	✓	✓

(continued on next page)

Table B1. Continued.

A		B		A		B		A		B		A		B			
C ₂ N	×	✓	C ₅ H ₂	×	✓	CCl ₂	×	×	Cu	✓	✓	N ₂ O ₅	×	✓	SiH ₂ O	×	✓
C ₂ N ₂	×	✓	C ₅ H ₂ N	×	×	CCl ₃	×	×	² H	×	✓	NF	✓	✓	SiH ₃	✓	✓
C ₂ O	×	✓	C ₅ H ₃	×	×	CCl ₄	✓	×	² H ₂	×	✓	NF ₂	✓	✓	SiH ₃ O	×	✓
C ₂ OH ₆	✓	✓	C ₅ H ₃ N	×	×	CF	✓	✓	² HC	×	×	NF ₃	✓	✓	SiH ₄	✓	✓
C ₂ P	×	✓	C ₅ H ₄	×	✓	CF ₂	✓	✓	² HCH ₂ NO	×	×	NH	✓	✓	SiHO	×	✓
C ₂ S	×	✓	C ₅ H ₅	×	×	CF ₃	✓	✓	² HCHO	×	✓	NH ₂	✓	✓	SiO	✓	✓
C ₂ Si	×	✓	C ₅ H ₆	×	×	CF ₃ I	×	×	² HHN	×	×	NH ₃	✓	✓	SiO ₂	×	✓
C ₃	✓	✓	C ₅ H ₇	×	×	CF ₃ I	×	×	² HN	×	×	NO	✓	✓	Ti	✓	×
C ₃ F ₄	×	×	C ₅ H ₈	×	×	CF ₃ O ₂	✓	×	F	✓	✓	NO ₂	✓	✓	Xe	✓	×
									F ₂	✓	✓	NO ₃	×	✓			

Table B2. Summary of negatively charged, unstateful species currently contained in QDB. Also given is the availability of electron collision data (column A) and heavy particle reaction rates (column B).

A		B		A		B		A		B		A		B	
Br ⁻	✓	✓	C ₅ N ⁻	×	✓	CN ⁻	×	✓	O ₃ ⁻	✓	✓				
C ⁻	×	✓	C ₆ ⁻	×	✓	Cl ⁻	✓	✓	O ₄ ⁻	×	✓				
C ₁₀ ⁻	×	✓	C ₆ H ⁻	×	✓	F ⁻	×	✓	OH ⁻	✓	✓				
C ₁₀ H ⁻	×	✓	C ₇ ⁻	×	✓	F ₂ ⁻	×	✓	S ⁻	×	✓				
C ₂ ⁻	×	✓	C ₇ H ⁻	×	✓	H ⁻	✓	✓	SF ₂ ⁻	×	×				
C ₂ H ⁻	×	✓	C ₈ ⁻	×	✓	N ₂ O ⁻	×	✓	SF ₃ ⁻	×	×				
C ₃ ⁻	×	✓	C ₈ H ⁻	×	✓	NF ₂ ⁻	×	×	SF ₄ ⁻	×	×				
C ₃ H ⁻	×	✓	C ₉ ⁻	×	✓	NF ₃ ⁻	×	×	SF ₅ ⁻	×	✓				
C ₃ N ⁻	×	✓	C ₉ H ⁻	×	✓	NH ₂ ⁻	×	✓	SF ₆ ⁻	×	✓				
C ₄ ⁻	×	✓	CF ₃ ⁻	✓	✓	NO ⁻	×	✓	SF ₆ ⁻	×	×				
C ₄ F ₈ ⁻	×	✓	CF ₄ ⁻	×	×	NO ₂ ⁻	×	✓	SiF ₃ ⁻	✓	×				
C ₄ H ⁻	×	✓	CH ⁻	×	✓	NO ₃ ⁻	×	✓	SiH ⁻	×	✓				
C ₅ ⁻	×	✓	CH ₂ ⁻	×	×	O ⁻	✓	✓	SiH ₂ ⁻	×	✓				
C ₅ H ⁻	×	✓	CH ₄ ⁻	×	×	O ₂ ⁻	×	✓	SiH ₃ ⁻	×	✓				

Finally, the free diffusion coefficient for positive ions is approximated by

$$D_+^{\text{free}} = \overline{D_{i+}^{\text{free}}}. \quad (\text{A.26})$$

Each *k*th species which is lost (or *stuck*) to the plasma boundary can get returned as *i*th species, introducing the boundary sources

$$\left(\frac{\delta n_i}{\delta t}\right)_{\text{diff}}^{\text{in}} = -\sum_k r_{ik} \left(\frac{\delta n_k}{\delta t}\right)_{\text{diff}}^{\text{out}} = \frac{A}{V} \sum_k \frac{D_k n_k s_k r_{ik}}{s_k \Lambda + \frac{4D_k}{v_k}}. \quad (\text{A.27})$$

Electron energy density balance equation:

The balance equation for the electron energy density consists of contributions from the absorbed external power, elastic and inelastic electron collisions, electron production and consumption and contribution from diffusion losses of electrons and ions.

$$\frac{d\varrho_e}{dt} = \frac{P}{V_e} - \left(\frac{\delta \varrho_e}{\delta t}\right)_{\text{el/inel}} - \left(\frac{\delta \varrho_e}{\delta t}\right)_{\text{gen/loss}} - \left(\frac{\delta \varrho_e}{\delta t}\right)_{\text{el} \rightarrow \text{walls}} - \left(\frac{\delta \varrho_e}{\delta t}\right)_{\text{ion} \rightarrow \text{walls}} \quad (\text{A.28})$$

Electron energy density loss rate due to electron collisions is described as

$$\left(\frac{\delta \varrho_e}{\delta t}\right)_{\text{el/inel}} = \sum_j R_j \Delta E_{e,j}, \quad (\text{A.29})$$

with the electron energy loss for *j*th reaction $\Delta E_{e,j}$ being

$$\Delta E_{e,j} = \begin{cases} \Delta E_{e,j}^{\text{inel}} & \text{inelastic collisions,} \\ 3 \frac{m_e}{M_{\text{cp},j}} (T_e - T_g) & \text{elastic collisions,} \\ 0 & \text{heavy species collisions or } a_{e,j}^{\text{R}} = 0, \end{cases} \quad (\text{A.30})$$

and

$$T_e = \frac{2}{3} \frac{\varrho_e}{n_e}. \quad (\text{A.31})$$

Rate of change of electron energy density due to generation and loss of electrons is described by

$$\left(\frac{\delta \varrho_e}{\delta t}\right)_{\text{gen/loss}} = \frac{3}{2} T_e \sum_j (a_{e,j}^{\text{R}} - a_{e,j}^{\text{L}}) R_j. \quad (\text{A.32})$$

Table B3. Summary of positively charged, unstateful species currently contained in QDB. Also given is the availability of electron collision data (column A) and heavy particle reaction rates (column B).

	A	B		A	B		A	B		A	B		A	B			
Al ⁺	✓	×	C ₂ P ⁺	✓	×	C ₄ Si ⁺	✓	×	CF ₃ ²⁺	×	×	² HH ₂ ⁺	×	×	N ₂ O ₂ ⁺	✓	✓
Ar ⁺	✓	✓	C ₂ S ⁺	✓	✓	C ₅ ⁺	✓	✓	CF ₃ I ⁺	×	×	F ⁺	✓	✓	N ₃ ⁺	✓	✓
Ar ²⁺	×	×	C ₂ Si ⁺	✓	✓	C ₅ H ⁺	✓	✓	CF ₄ ⁺	×	×	F ₂ ⁺	✓	✓	N ₄ ⁺	✓	✓
Ar ₂ ⁺	✓	✓	C ₃ ⁺	×	×	C ₅ H ₂ ⁺	✓	✓	CH ⁺	✓	✓	F ₂ O ⁺	×	×	NF ⁺	✓	✓
Ar ₃ ⁺	✓	✓	C ₃ ⁺	✓	✓	C ₅ H ₂ N ⁺	✓	✓	CH ⁺	✓	×	FSi ⁺	✓	×	NF ⁺	×	×
ArH ⁺	✓	✓	C ₃ F ⁺	×	×	C ₅ H ₃ ⁺	✓	✓	CH ²⁺	×	×	Fe ⁺	✓	✓	NF ₂ ⁺	✓	✓
B ⁺	✓	×	C ₃ F ₂ ⁺	×	×	C ₅ H ₃ N ⁺	✓	×	CH ₂ ⁺	✓	✓	H ⁺	✓	✓	NF ₂ ⁺	×	×
BCl ⁺	×	✓	C ₃ F ₃ ⁺	×	×	C ₅ H ₄ ⁺	✓	✓	CH ₂ F ⁺	×	×	H ₁₁ O ₅ ⁺	✓	✓	NF ₃ ⁺	✓	✓
BCl ₂ ⁺	✓	✓	C ₃ F ₄ ⁺	×	×	C ₅ H ₄ N ⁺	✓	×	CH ₂ F ₂ ⁺	×	×	H ₁₃ O ₆ ⁺	✓	✓	NF ₃ ⁺	×	×
BCl ₃ ⁺	✓	×	C ₃ F ₅ ⁺	✓	✓	C ₅ H ₅ ⁺	✓	✓	CH ₂ N ⁺	✓	✓	H ₁₅ O ₇ ⁺	✓	✓	NH ⁺	✓	✓
BF ⁺	✓	×	C ₃ F ₆ ⁺	✓	✓	C ₅ H ₅ N ⁺	×	×	CH ₂ NO ⁺	✓	×	H ₂ ⁺	✓	✓	NH ₂ ⁺	✓	✓
BF ₂ ⁺	✓	×	C ₃ F ₇ ⁺	✓	✓	C ₅ H ₇ ⁺	×	×	CH ₂ NS ⁺	✓	×	H ₂ ⁺	×	×	NH ₃ ⁺	✓	✓
BF ₃ ⁺	×	×	C ₃ F ₈	×	×	C ₅ H ₉ ⁺	×	×	CH ₂ O ⁺	×	✓	H ₂ ⁺	×	×	NH ₃ ⁺	×	×
Br ⁺	✓	✓	C ₃ H ⁺	✓	✓	C ₅ HN ⁺	✓	✓	CH ₂ O ₂ ⁺	✓	×	H ₂ F ⁺	✓	×	NH ₄ ⁺	✓	✓
Br ₂ ⁺	×	✓	C ₃ H ₂ ⁺	✓	✓	C ₅ HO ⁺	✓	×	CH ₂ P ⁺	✓	✓	H ₂ NO ⁺	✓	✓	NO ⁺	✓	✓
C ⁺	✓	✓	C ₃ H ₂ ⁺	×	×	C ₅ N ⁺	✓	✓	CH ₂ S ⁺	✓	×	H ₂ NO ₂ ⁺	✓	✓	NO ₂ ⁺	×	×
C ²⁺	×	×	C ₃ H ₂ N ⁺	✓	✓	C ₆ ⁺	✓	✓	CH ₂ Si ⁺	✓	✓	H ₂ NP ⁺	✓	×	NO ₂ ⁺	✓	✓
C ₁₀ ⁺	✓	✓	C ₃ H ₂ O ⁺	✓	×	C ₆ H ⁺	✓	✓	CH ₃ ⁺	✓	✓	H ₂ NSi ⁺	✓	✓	NP ⁺	✓	✓
C ₁₀ H ⁺	✓	✓	C ₃ H ₂ S ⁺	✓	×	C ₆ H ₂ ⁺	✓	✓	CH ₃ F ⁺	×	×	H ₂ Na ⁺	✓	×	NS ⁺	✓	✓
C ₁₀ H ₂ ⁺	✓	✓	C ₃ H ₂ Si ⁺	✓	✓	C ₆ H ₂ N ⁺	✓	×	CH ₃ N ⁺	×	×	H ₂ NaO ⁺	✓	×	NSi ⁺	✓	✓
C ₁₀ H ₂ N ⁺	✓	×	C ₃ H ₃ ⁺	✓	✓	C ₆ H ₃ ⁺	✓	✓	CH ₃ N ₂ ⁺	✓	×	H ₂ O ⁺	×	×	Na ⁺	✓	✓
C ₁₀ H ₃ ⁺	✓	✓	C ₃ H ₃ ⁺	×	×	C ₆ H ₄ ⁺	✓	✓	CH ₃ NS ⁺	×	×	H ₂ O ⁺	✓	✓	Ne ⁺	✓	×
C ₁₀ H ₆ ⁺	×	✓	C ₃ H ₃ N ⁺	✓	✓	C ₆ H ₄ N ⁺	✓	✓	CH ₃ O ⁺	✓	✓	H ₂ O ₃ ⁺	✓	✓	Ne ₂ ⁺	×	×
C ₁₀ HN ⁺	×	×	C ₃ H ₃ N ₂ ⁺	×	×	C ₆ H ₅ ⁺	✓	✓	CH ₃ O ₂ ⁺	✓	✓	H ₂ OP ⁺	✓	×	O ⁺	✓	✓
C ₁₀ N ⁺	✓	✓	C ₃ H ₃ O ⁺	✓	×	C ₆ H ₆ ⁺	×	✓	CH ₃ P ⁺	✓	×	H ₂ OSi ⁺	✓	×	O ²⁺	×	×
C ₁₁ ⁺	✓	×	C ₃ H ₃ S ⁺	✓	×	C ₆ H ₇ ⁺	✓	✓	CH ₃ S ⁺	✓	✓	H ₂ P ⁺	✓	✓	O ₂ ⁺	✓	✓
C ₁₂ H ₆ ⁺	×	×	C ₃ H ₄ ⁺	✓	✓	C ₆ H ₇ N ⁺	×	×	CH ₃ Si ⁺	✓	✓	H ₂ S ⁺	×	✓	O ₂ ⁺	×	×
C ₁₄ H ₁₀ ⁺	×	×	C ₃ H ₄ ⁺	✓	✓	C ₆ H ₈ N ⁺	×	×	CH ₄ ⁺	×	×	H ₂ S ⁺	✓	✓	O ₃ ⁺	×	×
C ₁₅ H ₉ ⁺	×	×	C ₃ H ₄ ²⁺	×	×	C ₆ HN ⁺	×	×	CH ₄ ⁺	✓	✓	H ₂ S ₂ ⁺	✓	✓	O ₄ ⁺	✓	✓
C ₂ ⁺	×	×	C ₃ H ₄ N ⁺	✓	✓	C ₆ HN ₂ ⁺	×	×	CH ₄ N ⁺	✓	×	H ₃ ⁺	✓	✓	OH ⁺	✓	✓
C ₂ ⁺	✓	✓	C ₃ H ₅ ⁺	✓	✓	C ₆ N ⁺	✓	✓	CH ₄ NO ⁺	✓	×	H ₃ NP ⁺	✓	×	OP ⁺	✓	×
C ₂ F ⁺	×	×	C ₃ H ₅ ⁺	×	×	C ₇ ⁺	✓	✓	CH ₄ NS ⁺	✓	×	H ₃ O ⁺	✓	✓	OS ⁺	✓	✓
C ₂ F ₂ ⁺	×	×	C ₃ H ₅ N ⁺	×	×	C ₇ H ⁺	✓	✓	CH ₄ O ⁺	✓	×	H ₃ OSi ⁺	✓	×	P ⁺	×	✓
C ₂ F ₃ ⁺	✓	✓	C ₃ H ₆ ⁺	✓	✓	C ₇ H ₂ ⁺	✓	✓	CH ₄ P ⁺	✓	×	H ₃ P ⁺	×	✓	PH ₃ ⁺	✓	✓
C ₂ F ₄ ⁺	✓	✓	C ₃ H ₆ N ⁺	×	✓	C ₇ H ₂ N ⁺	✓	✓	CH ₄ Si ⁺	✓	✓	H ₃ S ⁺	✓	✓	S ⁺	✓	✓
C ₂ F ₅ ⁺	✓	✓	C ₃ H ₆ O ⁺	✓	✓	C ₇ H ₃ ⁺	✓	✓	CH ₅ ⁺	✓	✓	H ₃ S ₂ ⁺	✓	✓	S ₂ ⁺	✓	✓
C ₂ F ₆	×	×	C ₃ H ₇ ⁺	✓	✓	C ₇ H ₃ N ⁺	✓	×	CH ₅ N ⁺	✓	×	H ₄ NO ₃ ⁺	✓	✓	SF ⁺	×	✓
C ₂ H ⁺	✓	✓	C ₃ H ₇ O ⁺	✓	×	C ₇ H ₄ ⁺	✓	✓	CH ₅ NS ⁺	×	×	H ₄ O ₂ ⁺	✓	✓	SF ₂ ⁺	×	✓
C ₂ H ²⁺	×	×	C ₃ H ₈ ⁺	✓	×	C ₇ H ₅ ⁺	✓	✓	CH ₅ O ⁺	✓	✓	H ₅ O ₂ ⁺	✓	✓	SF ₃ ⁺	×	✓
C ₂ H ₂ ⁺	×	×	C ₃ H ₉ ⁺	✓	×	C ₇ H ₇ ⁺	×	✓	CH ₅ S ⁺	✓	×	H ₅ Si ⁺	✓	✓	SF ₄ ⁺	×	✓
C ₂ H ₂ ⁺	✓	✓	C ₃ HN ⁺	✓	✓	C ₇ HN ⁺	✓	✓	CH ₆ N ⁺	✓	×	H ₆ NO ₄ ⁺	✓	✓	SF ₅ ⁺	×	✓
C ₂ H ₂ ²⁺	×	×	C ₃ HO ⁺	✓	×	C ₇ HO ⁺	✓	×	CH ₆ NS ⁺	✓	×	H ₇ O ₃ ⁺	✓	✓	SF ₆ ⁺	×	×
C ₂ H ₂ ²⁺	×	×	C ₃ HP ⁺	✓	×	C ₇ N ⁺	✓	✓	CHF ⁺	×	✓	H ₉ O ₄ ⁺	✓	✓	SO ₂ ⁺	×	×
C ₂ H ₂ N ⁺	✓	×	C ₃ HS ⁺	✓	✓	C ₈ ⁺	✓	✓	CHF ₂ ⁺	×	✓	HBr ⁺	×	×	SO ₂ ⁺	✓	✓
C ₂ H ₂ O ⁺	×	✓	C ₃ HSi ⁺	✓	✓	C ₈ H ⁺	✓	✓	CHNO ⁺	✓	✓	HBr ⁺	✓	✓	SSi ⁺	✓	✓
C ₂ H ₂ P ⁺	✓	×	C ₃ N ⁺	✓	✓	C ₈ H ₂ ⁺	✓	✓	CHNS ⁺	✓	×	HCHO ⁺	✓	✓	Si ⁺	✓	✓
C ₂ H ₂ S ⁺	✓	✓	C ₃ N ⁺	×	✓	C ₈ H ₂ N ⁺	✓	×	CHNSi ⁺	✓	✓	HCN ⁺	×	×	Si ₂ H ₂ ⁺	×	×
C ₂ H ₂ Si ⁺	✓	✓	C ₃ O ⁺	✓	✓	C ₈ H ₃ ⁺	✓	✓	CHO ⁺	✓	✓	HCN ⁺	✓	✓	Si ₂ H ₄ ⁺	×	✓
C ₂ H ₃ ⁺	✓	✓	C ₃ S ⁺	✓	✓	C ₈ H ₄ ⁺	✓	✓	CHO ₂ ⁺	✓	✓	HCP ⁺	✓	✓	Si ₂ H ₅ ⁺	×	×
C ₂ H ₃ N ⁺	✓	✓	C ₃ Si ⁺	✓	×	C ₈ H ₄ N ⁺	✓	✓	CHOS ⁺	✓	✓	HCl ⁺	✓	✓	Si ₂ H ₆ ⁺	×	×
C ₂ H ₃ NO ⁺	✓	×	C ₄ ⁺	✓	✓	C ₈ H ₅ ⁺	✓	×	CHP ⁺	×	✓	HF ⁺	✓	✓	SiCl ⁺	×	×
C ₂ H ₃ O ⁺	×	✓	C ₄ F ₄ ⁺	×	×	C ₈ H ₆ ⁺	×	✓	CHS ⁺	✓	✓	HF ⁺	×	×	SiCl ₂ ⁺	✓	×
C ₂ H ₃ P ⁺	✓	×	C ₄ F ₅ ⁺	×	×	C ₈ H ₇ ⁺	×	×	CHSi ⁺	✓	✓	HHe ⁺	✓	✓	SiCl ₃ ⁺	×	×
C ₂ H ₃ S ⁺	✓	×	C ₄ F ₆ ⁺	×	×	C ₈ HN ⁺	×	×	CN ⁺	✓	✓	HN ₂ O ⁺	✓	×	SiCl ₄ ⁺	×	×
C ₂ H ₃ Si ⁺	✓	✓	C ₄ F ₇ ⁺	✓	✓	C ₈ N ⁺	✓	✓	CNH ⁺	×	×	HNO ⁺	✓	✓	SiF ⁺	×	×
C ₂ H ₄ ⁺	✓	✓	C ₄ F ₈ ⁺	×	✓	C ₉ ⁺	✓	✓	CNO ⁺	✓	✓	HNP ⁺	✓	×	SiF ₂ ⁺	×	×
C ₂ H ₄ N ⁺	✓	×	C ₄ H ⁺	✓	✓	C ₉ H ⁺	✓	✓	CNS ⁺	×	×	HNS ⁺	✓	×	SiF ₃ ⁺	✓	×

(continued on next page)

Table B3. Continued.

	A	B		A	B		A	B		A	B		A	B		A	B
C ₂ H ₄ NO ⁺	✓	×	C ₄ H ₂ ⁺	✓	✓	C ₉ H ₂ ⁺	✓	✓	CNSi ⁺	✓	✓	HNSi ⁺	✓	✓	SiH ⁺	✓	✓
C ₂ H ₄ O ⁺	✓	×	C ₄ H ₂ N ⁺	✓	✓	C ₉ H ₂ N ⁺	✓	✓	CO ⁺	×	×	HO ₂ ⁺	✓	✓	SiH ₂ ⁺	✓	✓
C ₂ H ₄ O ₂ ⁺	✓	×	C ₄ H ₂ P ⁺	✓	×	C ₉ H ₃ ⁺	✓	✓	CO ⁺	✓	✓	HO ₂ S ⁺	✓	✓	SiH ₃ ⁺	✓	✓
C ₂ H ₄ P ⁺	✓	×	C ₄ H ₃ ⁺	✓	✓	C ₉ H ₃ N ⁺	✓	×	CO ²⁺	×	×	HO ₂ Si ⁺	✓	×	SiH ₃ N ⁺	✓	×
C ₂ H ₅ ⁺	✓	✓	C ₄ H ₃ N ⁺	✓	✓	C ₉ H ₄ ⁺	✓	✓	CO ₂ ⁺	×	×	HOP ⁺	✓	✓	SiH ₄ ⁺	✓	✓
C ₂ H ₅ ²⁺	×	×	C ₄ H ₄ ⁺	✓	✓	C ₉ H ₅ ⁺	✓	×	CO ₂ ²⁺	✓	✓	HOS ⁺	✓	✓	SiH ₄ ⁺	×	×
C ₂ H ₅ N ⁺	×	×	C ₄ H ₄ N ⁺	✓	✓	C ₉ H ₇ ⁺	×	×	CO ₂ ²⁺	×	×	HOSi ⁺	✓	✓	SiH ₄ N ⁺	✓	×
C ₂ H ₅ O ⁺	✓	✓	C ₄ H ₅ ⁺	✓	✓	C ₉ H ₈ ⁺	×	×	COF ₂ ⁺	×	×	HP ⁺	✓	✓	SiO ⁺	×	×
C ₂ H ₅ O ₂ ⁺	✓	×	C ₄ H ₅ N ⁺	×	×	C ₉ HN ⁺	✓	✓	CONH ₃ ⁺	×	×	HS ⁺	✓	✓	SiO ⁺	✓	✓
C ₂ H ₅ S ⁺	✓	×	C ₄ H ₆ ⁺	×	×	C ₉ HO ⁺	✓	×	COS ⁺	×	✓	HS ₂ ⁺	✓	✓	SiO ₂ ⁺	×	✓
C ₂ H ₆ ⁺	✓	✓	C ₄ H ₆ N ⁺	×	×	C ₉ N ⁺	✓	✓	COS ⁺	✓	×	HSSi ⁺	✓	✓	Ti ⁺	×	×
C ₂ H ₆ O ⁺	×	×	C ₄ H ₇ ⁺	✓	✓	CCl ⁺	✓	✓	CP ⁺	✓	✓	He ⁺	✓	✓	×e ⁺	✓	×
C ₂ H ₇ ⁺	✓	✓	C ₄ H ₈ ⁺	×	×	CCl ₂ ⁺	×	×	CS ⁺	×	✓	He ₂ ⁺	✓	✓	e ₂ ⁺	✓	×
C ₂ H ₇ O ⁺	✓	✓	C ₄ H ₉ ⁺	×	×	CCl ₂ ²⁺	×	×	CS ⁺	✓	✓	Hg ⁺	×	×			
C ₂ HN ⁺	✓	×	C ₄ HN ⁺	✓	✓	CCl ₃ ⁺	✓	×	CSi ⁺	✓	✓	I ⁺	×	×			
C ₂ HN ₂ ⁺	×	✓	C ₄ HN ₂ ⁺	×	×	CCl ₃ ²⁺	×	×	CaF ⁺	×	×	Kr ⁺	✓	×			
C ₂ HO ⁺	✓	×	C ₄ HO ⁺	✓	×	CClH ₂ ⁺	✓	×	CaF ⁺	✓	×	Kr ⁺	×	×			
C ₂ HP ⁺	✓	✓	C ₄ HP ⁺	✓	×	CF ⁺	×	×	CaF ²⁺	×	×	Mg ⁺	✓	✓			
C ₂ HS ⁺	✓	✓	C ₄ HS ⁺	✓	✓	CF ⁺	✓	✓	Cl ⁺	✓	✓	N ⁺	✓	✓			
C ₂ HSi ⁺	✓	✓	C ₄ HSi ⁺	✓	×	CF ₂ ⁺	×	×	Cl ₂ ⁺	✓	✓	N ²⁺	×	×			
C ₂ N ⁺	✓	✓	C ₄ N ⁺	✓	✓	CF ₂ ⁺	✓	✓	ClH ₂ ⁺	✓	✓	N ₂ ⁺	✓	✓			
C ₂ N ₂ ⁺	✓	✓	C ₄ N ₂ ⁺	×	×	CF ₂ ²⁺	×	×	CIO ⁺	✓	✓	N ₂ ⁺	×	×			
C ₂ O ⁺	✓	×	C ₄ P ⁺	✓	×	CF ₂ I ⁺	×	×	Cu ⁺	✓	✓	N ₂ H ⁺	✓	✓			
C ₂ OH ₆ ⁺	✓	×	C ₄ S ⁺	✓	✓	CF ₃ ⁺	✓	✓	² HH ⁺	✓	×	N ₂ O ⁺	✓	✓			

Table B4. Summary of the main acronyms used in the paper.

AcTC	Active thermochemical tables [15, 16]
API	Application program interface
BSR	B-spline R-matrix [66]
CCCBD	NIST computational chemistry comparison and benchmark database [26]
DBSR	Dirac B-spline R-matrix [67]
EEDF	Electron energy distribution functions
CRT	Chemistry reduction techniques
GUI	Graphical user interface
HPEM	Hybrid plasma equipment model [61]
ICP	Inductively coupled plasma
IP	Ionisation potential
LiDa	Lifetimes database
LoKI	Lisbon kinetics [87]
KIDA	Kinetic database for astrochemistry [5, 6]
ODE	Ordinary differential equations
PyGMol	Python global model
QDB	Quantemol database
QVT	Quantemol virtual tool
QGM	Quantemol global model
RMPS	R-matrix with pseudo-states [71]
RRS	Reduced reaction set
UDfA	UMIST database for astrochemistry [82]
ZDPlasKin	Zero-dimensional plasma kinetics solver [116]

Under a Maxwellian energy distribution assumption, each electron lost through the plasma boundary sheath takes away $2k_B T_e$ of energy with it [120], which gives

$$\left(\frac{\delta Q_e}{\delta t}\right)_{el \rightarrow walls} = -2T_e \left(\frac{\delta n_e}{\delta t}\right)_{walls} \quad (A.33)$$

The total charge flux is kept at zero, yielding

$$\left(\frac{\delta n_e}{\delta t}\right)_{walls} = \sum_i q_i \left(\frac{\delta n_i}{\delta t}\right)_{diff} \quad (A.34)$$

If it is assumed, that ions leave the plasma boundary sheath with the Bohm velocity, each positive ion removed from the

plasma takes away $\frac{1}{2}k_B T_e$ of kinetic energy, as well as sheath voltage acceleration energy [120].

$$\left(\frac{\delta \rho_e}{\delta t}\right)_{\text{ion} \rightarrow \text{walls}} = -\frac{1}{2}T_e \sum_{i_+} \left(\frac{\delta n_{i_+}}{\delta t}\right)_{\text{diff}} - \bar{V}_s \sum_{i_+} q_{i_+} \left(\frac{\delta n_{i_+}}{\delta t}\right)_{\text{diff}}. \quad (\text{A.35})$$

The last open parameter in the system is the mean sheath voltage \bar{V}_s , which, according to Lieberman and Lichtenberg [120], can be approximated by

$$\bar{V}_s = T_e \cdot \ln \left(\frac{\bar{M}_{i_+}}{2\pi m_e} \right)^{1/2}. \quad (\text{A.36})$$

This value of \bar{V}_s is only consistent with ICP plasma sources.

Appendix B. Summary of acronyms and species in QDB

Tables B1, B3 and B2 summarise the neutrals, anions and cations currently considered by QDB, respectively.

Table B4 summarises the main acronyms used in this paper.

ORCID iDs

Jonathan Tennyson  <https://orcid.org/0000-0002-4994-5238>

M Hanicinec  <https://orcid.org/0000-0003-3415-2996>

Carrick Smith  <https://orcid.org/0000-0002-2443-1425>

Luís L Alves  <https://orcid.org/0000-0002-2677-574X>

Klaus Bartschat  <https://orcid.org/0000-0001-6215-5014>

Annemie Bogaerts  <https://orcid.org/0000-0001-9875-6460>

Timo Gans  <https://orcid.org/0000-0003-1362-8000>

Andrew R Gibson  <https://orcid.org/0000-0002-1082-4359>

Satoshi Hamaguchi  <https://orcid.org/0000-0001-6580-8797>

Kathryn R Hamilton  <https://orcid.org/0000-0002-8245-0122>

Christian Hill  <https://orcid.org/0000-0001-6604-0126>

Shahid Rauf  <https://orcid.org/0000-0001-5689-6115>

Kevin van 't Veer  <https://orcid.org/0000-0003-2540-467X>

Oleg Zatsarinny  <https://orcid.org/0000-0001-8253-883X>

References

- [1] Bartschat K and Kushner M J 2016 *Proc. Natl Acad. Sci. USA* **113** 7026–34
- [2] Pitchford L C et al 2017 *Plasma Process. Polym.* **14** 1600098
- [3] Emoto M, Murakami I, Kato D, Yoshida M, Kato M and Imazu S 2019 *Atoms* **7** 91
- [4] Park J H, Choi H, Chang W S, Chung S Y, Kwon D C, Song M Y and Yoon J S 2020 *Appl. Sci. Converg. Technol.* **29** 5–9
- [5] Wakelam V et al 2012 *Astrophys. J. Suppl.* **199** 21
- [6] Wakelam V et al 2015 *Astrophys. J. Suppl.* **217** 20
- [7] Celiberto R et al 2016 *Plasma Sources Sci. Technol.* **25** 033004
- [8] Adamovich I et al 2017 *J. Phys. D: Appl. Phys.* **50** 323001
- [9] Adamovich I et al 2022 *J. Phys. D: Appl. Phys.* **55** 373001
- [10] Tennyson J et al 2017 *Plasma Sources Sci. Technol.* **26** 055014
- [11] Hill C 2019 *Technical Meeting on the Development of Software Programs and Database Tools for Modelling Edge Plasma Processes in Fusion Devices; Appendix 5: Draft Standards for the Representation of Atomic and Molecular Species and States in Databases Tech. Rep.* (IAEA) <https://nds.iaea.org/publications/indc/indc-nds-0805.pdf>
- [12] Hill C 2019 PyValem: a Python package for parsing, validating, manipulating and interpreting the chemical formulas, quantum states and labels of atoms, ions and small molecules <https://github.com/xnx/pyvalem>
- [13] Bernath P F 2015 *Spectra of Atoms and Molecules* 3rd edn (Oxford: Oxford University Press)
- [14] Tennyson J 2019 *Astronomical Spectroscopy: An Introduction to the Atomic and Molecular Physics of Astronomical Spectra* 3rd edn (Singapore: World Scientific)
- [15] Ruscic B, Pinzon R E, Morton M L, von Laszewski G, Bittner S J, Nijssure S G, Amin K A, Minkoff M and Wagner A F 2004 *J. Phys. Chem. A* **108** 9979–97
- [16] Ruscic B, Feller D and Peterson K A 2014 *Theor. Chem. Acc.* **133** 1415
- [17] Chase M W, Davies C A, Downey J R, Frurip D J, McDonald R A and Syverud A N 1985 *J. Phys. Chem. Ref. Data* **14** 1–926 <https://srdata.nist.gov/JPCRD/jpcrdS1V14.pdf>
- [18] Burcat A 1984 *Combustion Chemistry* ed W Gardiner (New York: Springer)
- [19] McBride B J, Zehe M J and Gordon S 2002 *NASA Glenn Coefficients for Calculating Thermodynamic Properties of Individual Species Tech. Rep. 2002-211556* (NASA)
- [20] Barklem P S and Collet R 2016 *Astron. Astrophys.* **588** A96
- [21] Gamache R R et al 2017 *J. Quant. Spectrosc. Radiat. Transfer* **203** 70–87
- [22] Tennyson J et al 2020 *J. Quant. Spectrosc. Radiat. Transfer* **255** 107228
- [23] Gamache R R, Vispoel B, Rey M, Nikitin A, Tyuterev V, Egorov O, Gordon I E and Boudon V 2021 *J. Quant. Spectrosc. Radiat. Transfer* **271** 107713
- [24] Svehla R A 1962 *Estimated Viscosities and Thermal Conductivities of Gases at High Temperature Tech. Rep. 1962-01-01T00:00:00Z* (Cleveland: National Aeronautics and Space Administration Lewis Research Center)
- [25] Hirschfelder J O, Curtiss C F and Bird R B 1966 *The Molecular Theory of Gases and Liquids* (Hoboken, NJ: Wiley-Interscience)
- [26] Johnson R D III 1999 *Computational Chemistry Comparison and Benchmark Database Tech. Rep. 101 NIST* https://nist.gov/publications/nist-101-computational-chemistry-comparison-and-benchmark-database?pub_id=831580
- [27] Hill C, Dubernet M L, Endres C, Karwasz G, Marinković B, Marquart T, Heinola K, Zwolf C M and Moreau N 2021 *Classification of Processes in Plasma Physics Tech. Rep. Version 2.2* (International Atomic Energy Agency) <https://amdis.iaea.org/databases/processes>
- [28] Thoman J W, Suzuki K, Kable S H and Steinfeld J I 1986 *J. Appl. Phys.* **60** 2775–7
- [29] Booth J P, Hancock G, Perry N D and Toogood M J 1989 *J. Appl. Phys.* **66** 5251–7
- [30] Booth J P and Sadeghi N 1991 *J. Appl. Phys.* **70** 611–20
- [31] Miyata K, Hori M and Goto T 1997 *Japan. J. Appl. Phys. I* **36** 5340
- [32] Matsuda A, Nomoto K, Takeuchi Y, Suzuki A, Yuuki A and Perrin J 1990 *Surf. Sci.* **227** 50–6
- [33] Hikosaka Y, Toyoda H and Sugai H 1993 *Japan. J. Appl. Phys.* **2** **32** L690
- [34] Matsushita J, Sasaki K and Kadota K 1997 *Japan. J. Appl. Phys. I* **36** 4747

- [35] Tatsumi T, Hikosaka Y, Morishita S, Matsui M and Sekine M 1999 *J. Vac. Sci. Technol. A* **17** 1562–9
- [36] Gomez S, Steen P G and Graham W G 2002 *Appl. Phys. Lett.* **81** 19–21
- [37] Zhang D and Kushner M J 2000 *J. Vac. Sci. Technol. A* **18** 2661–8
- [38] Huang S, Volynets V, Hamilton J R, Nam S K, Song I C, Lu S, Tennyson J and Kushner M J 2018 *J. Vac. Sci. Technol. A* **36** 021305
- [39] Marcos G, Rhallabi A and Ranson P 2003 *J. Vac. Sci. Technol. A* **21** 87–95
- [40] Sankaran A and Kushner M J 2004 *J. Vac. Sci. Technol. A* **22** 1260–74
- [41] Huard C M, Zhang Y, Sriraman S, Paterson A and Kushner M J 2017 *J. Vac. Sci. Technol. A* **35** 05C301
- [42] Zhang D and Kushner M J 2001 *J. Vac. Sci. Technol. A* **19** 524–38
- [43] Hamaguchi S and Dalvie M 1994 *J. Vac. Sci. Technol. A* **12** 2745–53
- [44] Mayo A A, Hamaguchi S, Joo J H and Rossnagel S M 1997 *J. Vac. Sci. Technol. B* **15** 1788–93
- [45] Yamamura Y, Takiguchi T and Tawara H 1990 *Research Report, National Institute for Fusion Science-DATA Series, NIFS-DATA-1*
- [46] Yamamura Y and Tawara H 1996 *At. Data Nucl. Data Tables* **62** 149253
- [47] Behrisch R and Eckstein W (ed) 2007 *Sputtering by Particle Bombardment* (Berlin: Springer)
- [48] 2022 Institute of Applied Physics TU Wien A simple Sputter yield calculator <https://www.iap.tuwien.ac.at/www/surface/sputteryield> (accessed 22 September 2022)
- [49] Kino H, Ikuse K, Dam H C and Hamaguchi S 2021 *Phys. Plasmas* **28** 013504
- [50] Ikuse K 2022 *GPR-based Sputtering Yield Prediction* <https://www-camt.eng.osaka-u.ac.jp/hamaguchi/SY/> (accessed 22 September 2022)
- [51] Tomlin A S, Pilling M J, Turányi T, Merkin J H and Brindley J 1992 *Combust. Flame* **91** 107–30
- [52] Gorban A 2018 *Curr. Opin. Chem. Eng.* **21** 48–59
- [53] Tomlin A S, Turányi T and Pilling M J 1997 *Comprehensive Chemical Kinetics* vol 35 (New York: Elsevier) pp 293–437
- [54] Okino M S and Mavrouniotis M L 1998 *Chem. Rev.* **98** 391–408
- [55] Law C K 2007 *Proc. Combust. Inst.* **31** 1–29
- [56] Lu T and Law C K 2009 *Prog. Energy Combust. Sci.* **35** 192–215
- [57] Sun S R, Wang H X and Bogaerts A 2020 *Plasma Sources Sci. Technol.* **29** 025012
- [58] Venot O, Bounaceur R, Dobrijevic M, Hébrard E, Cavalié T, Tremblin P, Drummond B and Charnay B 2019 *Astron. Astrophys.* **624** A58
- [59] Hanicinc M, Mohr S and Tennyson J 2020 *Plasma Sources Sci. Technol.* **29** 125024
- [60] Rockwood S D 1973 *Phys. Rev. A* **8** 2348–58
- [61] Kushner M J 2009 *J. Phys. D: Appl. Phys.* **42** 194013
- [62] COMSOL AB COMSOL multiphysics (Stockholm, Sweden) <http://comsol.com>
- [63] Kee R J et al 2000 *CHEMKIN Collection* (San Diego, CA: Reaction Design, Inc.)
- [64] Stout P J, Yang H Q, Dionne P, Leonard A, Tan Z, Przekwas A J and Krishnan A 1999 *Design, Test, and Microfabrication of MEMS and MOEMS* vol 3680 ed B Courtois, S B Cray, W Ehrfeld, H Fujita, J M Karam, K W Markus and W Ehrfeld (Bellingham, Wash., USA: International Society for Optics and Photonics (SPIE)) pp 328–39
- [65] Esgee Technologies, Inc. 2015 *VizGlow: Plasma Modeling Software for Multi-Dimensional Simulations of Non-Equilibrium Glow Discharge Systems, Theory Manual, Version 2.1* (San Diego, CA, USA)
- [66] Zatsarinny O 2006 *Comput. Phys. Commun.* **174** 273–356
- [67] Zatsarinny O and Bartschat K 2008 *Phys. Rev. A* **77** 062701
- [68] Zatsarinny O and Bartschat K 2013 *J. Phys. B: At. Mol. Opt. Phys.* **46** 112001
- [69] Zatsarinny O 2021 <https://github.com/zatsaroi>
- [70] Schneider B I et al 2022 AMP gateway: a portal for research and education in atomic and molecular physics <https://ampgateway.org/>
- [71] Bartschat K, Hudson E T, Scott M P, Burke P G and Burke V M 1996 *J. Phys. B: At. Mol. Opt. Phys.* **29** 115–23
- [72] Zatsarinny O and Bartschat K 2009 *Phys. Scr. T* **134** 014020
- [73] Zatsarinny O, Wang Y and Bartschat K 2014 *Phys. Rev. A* **89** 022706
- [74] Zatsarinny O and Bartschat K 2012 *Phys. Rev. A* **85** 062710
- [75] Zatsarinny O and Bartschat K 2006 *J. Phys. B: At. Mol. Opt. Phys.* **39** 2145–58
- [76] Allan M, Zatsarinny O and Bartschat K 2011 *J. Phys. B: At. Mol. Opt. Phys.* **44** 065201
- [77] Zatsarinny O and Bartschat K 2010 *J. Phys. B: At. Mol. Opt. Phys.* **43** 074031
- [78] Fursa D V and Bray I 1995 *Phys. Rev. A* **52** 1279–97
- [79] Hudson E T, Bartschat K, Scott M P, Burke P G and Burke V M 1996 *J. Phys. B: At. Mol. Opt. Phys.* **29** 5513–26
- [80] Bartschat K 1998 *J. Phys. B: At. Mol. Opt. Phys.* **31** L469–76
- [81] Zatsarinny O and Bartschat K 2012 *Phys. Rev. A* **85** 062709
- [82] McElroy D, Walsh C, Markwick A J, Cordiner M A, Smith K and Millar T J 2013 *Astron. Astrophys.* **550** A36
- [83] Goebel D M and Katz I 2008 *Fundamentals of Electric Propulsion: Ion and Hall Thrusters* (California: JPL)
- [84] Smith T D, Kamhawi H, Hickman T, Haag T, Dankanich J, Plozin K, Byrne L and Szabo J 2016 *Overview of NASA Iodine Hall Thruster Propulsion System Development Tech. Rep.* (NASA) <https://ntrs.nasa.gov/api/citations/20160006296/downloads/20160006296.pdf>
- [85] Kaganovich I D et al 2020 *Phys. Plasmas* **27** 120601
- [86] Ambalampitiya H B, Hamilton K R, Zatsarinny O, Bartschat K, Turner M A P, Dzarasova A and Tennyson J 2021 *Atoms* **9** 103
- [87] Guerra V, Tejero-del-Caz A, Pintassilgo C D and Alves L L 2019 *Plasma Sources Sci. Technol.* **28** 073001
- [88] Tejero-del-Caz A, Guerra V, Gonçalves D, da Silva M L, Marques L, Pinhão N, Pintassilgo C D and Alves L L 2019 *Plasma Sources Sci. Technol.* **28** 043001 (see <https://nprime.tecnico.ulisboa.pt/loki/>)
- [89] Tejero-del-Caz A, Guerra V, Pinhão N, Pintassilgo C D and Alves L L 2021 *Plasma Sources Sci. Technol.* **30** 065008
- [90] Coche P, Guerra V and Alves L L 2016 *J. Phys. D: Appl. Phys.* **49** 235207 (see <https://github.com/IST-Lisbon/LoKI>)
- [91] Stoffels E, Stoffels W W, Vender D, Haverlag M, Kroesen G M W and de Hoog F J 1995 *Contrib. Plasma Phys.* **35** 331–57
- [92] Wilke C R 1950 *Chem. Eng. Prog.* **46** 95–104
- [93] Huang S, Volynets V, Hamilton J R, Lee S, Song I C, Lu S, Tennyson J and Kushner M J 2017 *J. Vac. Sci. Technol. A* **35** 031302
- [94] Hamilton J R, Tennyson J, Huang S and Kushner M J 2017 *Plasma Sources Sci. Technol.* **26** 065010
- [95] Agarwal A, Bera K, Kenney J, Likhanskii A and Rauf S 2017 *J. Phys. D: Appl. Phys.* **50** 424001
- [96] Weller H G, Tabor G, Jasak H and Fureby C 1998 *Comput. Phys.* **12** 620–31
- [97] Kimura T and Hanaki K 2008 *Japan. J. Appl. Phys.* **47** 8546–52
- [98] Schröter S et al 2018 *Phys. Chem. Chem. Phys.* **20** 24263
- [99] Brisset A, Gibson A, Schröter S, Niemi K, Booth J P, Gans T, O’Connell D and Wagenaars E 2021 *J. Phys. D: Appl. Phys.* **54** 285201
- [100] Lietz A M and Kushner M J 2016 *J. Phys. D: Appl. Phys.* **49** 425204

- [101] Schröter S, Bredin J, Gibson A R, West A, Dedrick J P, Wagenaars E, Niemi K, Gans T and O'Connell D 2020 *Plasma Sources Sci. Technol.* **29** 105001
- [102] Vervloessem E, Aghaei M, Jardali F, Hafezkhiani N and Bogaerts A 2020 *ACS Sustain. Chem. Eng.* **8** 9711–20
- [103] Jardali F, Van Alphen S, Creel J, Ahmadi Eshtehardi H, Axelsson M, Ingels R, Snyders R and Bogaerts A 2021 *Green Chem.* **23** 1748–57
- [104] Van Alphen S, Jardali F, Creel J, Trenchev G, Snyders R and Bogaerts A 2021 *Sustain. Energy Fuels* **5** 1786–800
- [105] Pattyn C, Maira N, Remy A, Roy N C, Iseni S, Petitjean D and Reniers F 2020 *Phys. Chem. Chem. Phys.* **22** 24801–12
- [106] Adamovich I V, Macheret S O, Rich J W and Treanor C E 1998 *J. Thermophys. Heat Transfer* **12** 57–65
- [107] Esposito F, Armenise I and Capitelli M 2006 *Chem. Phys.* **331** 1–8
- [108] Esposito F, Armenise I, Capitta G and Capitelli M 2008 *Chem. Phys.* **351** 91–8
- [109] Terraz L, Silva T, Morillo-Candas A, Guaitella O, Tejero-del-Caz A T, Alves L L and Guerra V 2019 *J. Phys. D: Appl. Phys.* **53** 094002
- [110] Guerra V and Loureiro J 1995 *J. Phys. D: Appl. Phys.* **28** 1903–18
- [111] Gordiets B and Ricard A 1993 *Plasma Sources Sci. Technol.* **2** 158–63
- [112] McNeal R J, Whitson M E Jr and Cook G R 1974 *J. Geophys. Res.* **79** 1527–31
- [113] Eckstrom D J 1973 *J. Chem. Phys.* **59** 2787–95
- [114] Breshears W D and Bird P F 1968 *J. Chem. Phys.* **48** 4768–73
- [115] Pancheshnyi S, Eismann B, Hagelaar G J M and Pitchford L C 2008 *Computer Code ZDPlasKin, LAPLACE, CNRS-UPS-INP* (Toulouse: University of Toulouse) <http://zdplaskin.laplace.univ-tlse.fr>
- [116] Hagelaar G J M and Pitchford L C 2005 *Plasma Sources Sci. Technol.* **14** 722–33
- [117] van 't Veer K, Engelmann Y, Reniers F and Bogaerts A 2020 *J. Phys. Chem. C* **124** 22871–83
- [118] Schröter S, Gibson A R, Kushner M J, Gans T and O'Connell D 2018 *Plasma Phys. Control. Fusion* **60** 014035
- [119] Lee C and Lieberman M A 1995 *J. Vac. Sci. Technol. A* **13** 368–80
- [120] Lieberman M A and Lichtenberg A J 2005 *Principles of Plasma Discharges and Materials Processing* 2nd edn (Hoboken, NJ: Wiley-Interscience)